DISSERTATION

POWER CONVERSION AND CONTROL FOR PULSED MAGNETRON REACTIVE SPUTTERING

Submitted by

David John Christie

Department of Electrical and Computer Engineering

In partial fulfillment of the requirements

For the Degree of Doctor of Philosophy

Colorado State University

Fort Collins, Colorado

Spring 2004

Reproduced with permission of the copyright owner. Further reproduction prohibited without permission.

UMI Number: 3131662

Copyright 2004 by
Christie, David John

All rights reserved.

INFORMATION TO USERS

The quality of this reproduction is dependent upon the quality of the copy submitted. Broken or indistinct print, colored or poor quality illustrations and photographs, print bleed-through, substandard margins, and improper alignment can adversely affect reproduction.

In the unlikely event that the author did not send a complete manuscript and there are missing pages, these will be noted. Also, if unauthorized copyright material had to be removed, a note will indicate the deletion.

UMI®

UMI Microform 3131662
Copyright 2004 by ProQuest Information and Learning Company.
All rights reserved. This microform edition is protected against
unauthorized copying under Title 17, United States Code.

ProQuest Information and Learning Company
300 North Zeeb Road
P.O. Box 1346
Ann Arbor, MI 48106-1346

Reproduced with permission of the copyright owner. Further reproduction prohibited without permission.

Copyright by David John Christie 2004

All Rights Reserved

Reproduced with permission of the copyright owner. Further reproduction prohibited without permission.

COLORADO STATE UNIVERSITY

February 26, 2004

WE HEREBY RECOMMEND THAT THE DISSERTATION PREPARED UNDER OUR SUPERVISION BY DAVID JOHN CHRISTIE ENTITLED POWER CONVERSION AND CONTROL FOR PULSED MAGNETRON REACTIVE SPUTTERING BE ACCEPTED AS FULFILLING IN PART REQUIREMENTS FOR THE DEGREE OF DOCTOR OF PHILOSOPHY.

Committee on Graduate Work

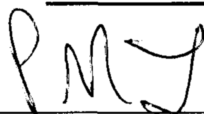

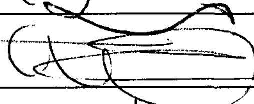

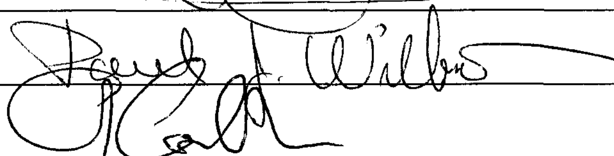

Adviser

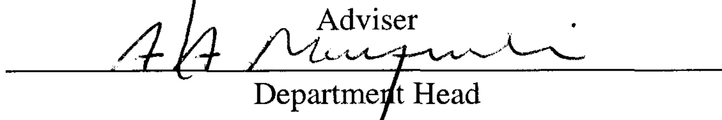

Department Head

Reproduced with permission of the copyright owner. Further reproduction prohibited without permission.

ABSTRACT OF DISSERTATION

POWER CONVERSION AND CONTROL FOR PULSED MAGNETRON REACTIVE SPUTTERING

The application of reactive sputtering is pervasive in the field of thin film coatings. This dissertation addresses process dynamics during and after arc response shutdown, dual magnetron reactive co-sputtering process control requirements, and pulsed power supply requirements for high power pulsed magnetron sputtering (HPPMS).

In reactive sputtering processes, the flux of target atoms to chamber surfaces is shut off when the power supply output turns off for arc handling. This causes the partial pressure of the reactive gas to rise. It is necessary to respond quickly to an arc in order to keep gas pressure within an acceptable range. The partial pressure variation, target and chamber surface coverage fractions, and deposition rate when process power is re-established, may be estimated with a simple dynamical process simulation model. This can provide guidance for arc detection and response time scale requirements for transition mode operation. A representative large area reactive coating process is simulated to explore arc response time guidelines.

Pulsed current source supplies can independently regulate power delivered to each magnetron in a dual magnetron sputtering arrangement. This enables reactive co-sputtering of optical films when one target material is different than the other. Modeling shows that reactive gas partial pressure must be regulated, in addition to independent

Reproduced with permission of the copyright owner. Further reproduction prohibited without permission.

regulation of power to each target, in order to gain control over film composition. This is confirmed by experiment. Optical films having a customized index of refraction were deposited by dual magnetron reactive co-sputtering, with independent regulation of the power delivered to each target. Reactive gas partial pressure was regulated by using a mass spectrometer as the partial pressure sensor.

HPPMS has created growing interest because of its ability to generate dense plasma with high target material ion content, using essentially conventional magnetron sputtering equipment. However, HPPMS is also capable of delivering large energies to unavoidable process arcs. Unless properly handled, arcs can generate macro-particles and target damage, limiting the usefulness of the technique. However, coatings quite suitable for industrial applications may be applied if the pulsed supply incorporates arc handling. A novel arc handling topology with energy recycling is proposed. Simulation and experiments with representative hardware both confirm operation of the topology. An experimental power supply incorporating this arc handling topology, capable of peak powers up to 3 megawatts and peak currents to 3000 A, at discharge voltages reaching 2 kV, has been designed and constructed. This new power supply technology enables the practical application of a whole new range of sputtering processes. These processes can exploit the flux of ionized target material from essentially conventional magnetron sputtering equipment to deposit dense equi-axed films.

The HPPMS power supply performance was experimentally verified by driving large and small magnetron loads. Temporal current and voltage waveforms are shown for normal and arcing operation. In addition, this power supply has been used in collaborative efforts to enable HPPMS deposition of high density (2.7 g/cm^3)

Reproduced with permission of the copyright owner. Further reproduction prohibited without permission.

thin (<200 Å) carbon films and HPPMS reactive sputtering deposition of dielectric films on dielectric substrates.

David John Christie
Department of Electrical and Computer Engineering
Colorado State University
Fort Collins, CO 80523
Spring 2004

Reproduced with permission of the copyright owner. Further reproduction prohibited without permission.

Acknowledgements

My wife Claudia and my children Brian, Kathleen, and Heather were very patient during my graduate studies at Colorado State University. Their love and support kept me going.

My adviser George Collins encouraged me to start and challenged me to go beyond myself and make it happen.

Bill Sproul made numerous insightful observations, engaged in many helpful discussions, and gave many useful suggestions. He also reviewed the draft of this dissertation. Thanks Bill!

I would like to thank the folks at Advanced Energy for their support and encouragement, especially Rich and Brenda Scholl, Randy Heckman, Tim Kerr, Geoff Drummond, Hendrik Walde, George McDonough, and Holly Caswell. Several people at Advanced Energy helped with experiments one way or another. They include Dan Carter, Fernando Tomasel, Karen Peterson, Randy Grilley, Bill Goldsworth, Chuck Miller, John Accardo, and Dan Doran.

Ben DeKoven, Pat Ward, Bob Weiss of Intevac and André Anders of LBL did an amazing job on the HPPMS carbon film development in a very short time. John Davis and Michael Stowell of AFC performed numerous HPPMS large area reactive sputtering experiments.

Reproduced with permission of the copyright owner. Further reproduction prohibited without permission.

Dedication

To Mom and Dad, who expected my best, and to the visionaries who believed in me and recruited me to solve interesting and challenging technical problems.

Reproduced with permission of the copyright owner. Further reproduction prohibited without permission.

TABLE OF CONTENTS

CHAPTER 1 INTRODUCTION 1
1.1 Background 1
1.2 Reactive Sputtering Arc Response Dynamics 5
1.3 Pulsed Reactive Co-sputtering 6
1.4 HPPMS Power Supplies for Reactive Sputtering 9
1.5 References 15
CHAPTER 2 REACTIVE SPUTTERING ARC RESPONSE DYNAMICS 17
2.1 Approach 17
2.2 Static Model 17
2.3 Dynamical Model 23
2.4 Simulations of Arc Response Dynamics 29
2.5 Arc Response Requirements 37
2.6 Summary and Conclusions 40
2.7 References 40
CHAPTER 3 PULSED REACTIVE CO-SPUTTERING 41
3.1 Approach 41
3.2 Modeling 42
3.3 Experimental conditions 53
3.4 Results and Discussion 55
3.5 Conclusions 59
3.6 References 60
CHAPTER 4 POWER SUPPLIES FOR HIGH POWER PULSED REACTIVE SPUTTERING 61
4.1 Approach 61
4.2 Discharge Circuit Design Considerations 62
4.3 Modifications for Arc Handling 74
4.4 Experimental Conditions 85
4.5 Results and Discussion 88
4.6 Process Results Enabled by the Experimental Pulsed Power Supply 93
4.7 Summary 96
4.8 References 96
CHAPTER 5 SUMMARY AND FUTURE WORK 97
5.1 Perspective 97
5.2 Reactive Sputtering Arc Response Dynamics 97
5.3 Pulsed Reactive Co-Sputtering 98
5.4 HPPMS Power Supplies for Reactive Sputtering 99
5.5 Integration of HPPMS, Reactive Co-sputtering, and Arc Response Dynamics ... 100
APPENDIX A EXPONENTIAL VOLTAGE – CURRENT CHARACTERISTIC SIMULATION 102

Reproduced with permission of the copyright owner. Further reproduction prohibited without permission.

CHAPTER 1

INTRODUCTION

1.1 Background

The application of thin film coatings is truly pervasive. They have found broad application in products used by essentially the whole cross section of society on a daily basis. Their use has increased to the point where essentially everyone in technically developed societies uses products incorporating thin film coatings, or products that are made with tools and equipment incorporating thin film coatings. These applications include the aluminum coating on Compact Disks®, the TiN wear coating on drill bits and industrial cutting tools, SiO_2 oxygen barrier coatings on food packaging, and low-e coatings on architectural and automotive glass.[1,2] Low-e coatings make buildings more energy efficient, more pleasant, and more attractive, and gold colored TiN coatings on drill bits extend their life three to four times.

One common technique for depositing these coatings is sputtering.[3] The sputtering process is depicted schematically in Figure 1.1.1. In this case, aluminum is being sputtered by argon ions and deposited on a work piece. Ar^+ ions impact the target surface, causing atoms to be "sandblasted" away at the atomic level. These target atoms then propagate to the work piece, where they condense on the surface, much like steam condenses on the mirror in the shower room. It is important to note that the ionization fraction of the sputtered atoms is on the order of one percent, very low, so transport of

Reproduced with permission of the copyright owner. Further reproduction prohibited without permission.

these atoms is not affected by electric or magnetic fields to a significant degree. Transport is dominated by gas kinetics and collisions in the molecular flow regime for practical sputter deposition processes.[4]

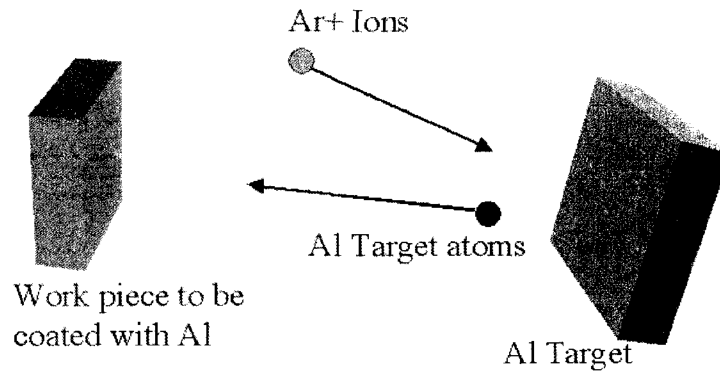

Figure 1.1.1. Schematic diagram of the sputtering process.

The sputtering process can be modified by the addition of reactive gas, to deposit films composed of the reactive product of the gas and the target material. This is called reactive sputtering. Figure 1.1.2 is a schematic depiction of the reactive sputtering process in which SiO_2 is formed. In the diagram, the elemental Si from the target reacts with O_2 to form SiO_2 at the target surface. The O_2 is delivered by the natural flux to the target surface, determined by molecular flow gas kinetics, governed by pressure, temperature, and mass of the molecules.

Reproduced with permission of the copyright owner. Further reproduction prohibited without permission.

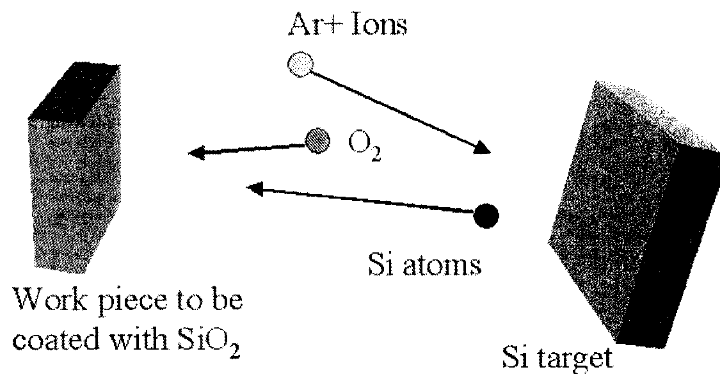

Figure 1.1.2. Simple diagram of the reactive sputtering process.

Reactive sputtering is now commonly used to deposit compounds formed from sputtered target material and one or more reactive gases. These films offer many advantages but the process is difficult to control, due to its highly non-linear nature and essentially un-measurable fundamental parameters, such as coverage fraction and ion flux.

Reactive sputtering has proven to be a useful technique for depositing a wide range of compounds, including TiN, TiO_2, SiO_2, Si_3N_4, SnO_2, ZnO, and Al_2O_3, which are in common industrial use. Films of these compounds find applications in anti-reflective coatings, first surface mirrors, solar control coatings, automotive glass, architectural glass, hard coatings on tools and turbine engine blades, decorative coatings, and "life-time" coatings on plumbing fixtures, just to name a few. Control of these processes has, however, proven difficult, due largely to extreme non-linearities, driven by un-measurable parameters.

Reproduced with permission of the copyright owner. Further reproduction prohibited without permission.

Feedback control approaches have been developed using various means to assess the state of the process. Optical feedback from the plasma has been used with some success, focusing primarily on a target material emission line.[5] However, maintaining near absolute calibration over time is problematic, since the optical surfaces tend to be coated over time, changing their transmission. Voltage feedback has also been used with some success, using the process voltage for feedback.[6] This approach is subject to changing anode voltage drop, due in particular to the anode becoming partially coated with dielectric from the process. Feedback from a mass spectrometer has also been applied with considerable success, especially in the fields of hard coatings for cutting tools and tribological coatings.[7,8,9,10] This approach has the fundamental advantage of measuring reactive gas partial pressure directly, hence controlling the flux of reactive gas to the target and chamber surfaces directly. It has the added advantage that periodic calibration of the mass spectrometer is possible with reference gases and independent pressure gauges.

Process control issues have motivated workers in the field to develop process models to aid in the understanding of the issues, with the hope that process control and performance would be enhanced. Of course, the desired outcome is broader application of these coatings, at lower and lower costs.

The objective of the research effort described herein was to advance the state of reactive sputtering. Even though it is a maturing technique, there is still ample room to advance the state of knowledge by modeling and experimentation. This dissertation addresses reactive sputtering process stability issues associated with arc handling, pulsed

Reproduced with permission of the copyright owner. Further reproduction prohibited without permission.

dual magnetron reactive co-sputtering, and power supplies for high peak power reactive magnetron sputtering. New results were obtained in each of the three areas.

1.2 Reactive Sputtering Arc Response Dynamics

One consideration of paramount importance is the stability of the reactive sputtering process. Stability can have broad meaning. There is on one hand the intrinsic stability, which often implies freedom from oscillation, or perhaps, the ability to stay within a bound-able neighborhood of a desired operating point. While this notion of stability is quite applicable, and important, to reactive sputtering processes, there is another notion of stability which must be also considered. Reactive sputtering processes are by their nature prone to arcing. The dielectric material which forms on the target surface in some processes is believed to accumulate electrical charge to the point where it breaks down and initiates an arc from the plasma to the target, where the glow discharge over much of the target surface collapses to a small diameter arc.[11] Periodic reversal of the voltage applied to the process to discharge the dielectric on the target surface has been shown to reduce the occurrence of arcing. When an arc does occur, it must be handled by the system power supply. This typically entails an interruption in the power delivered to the process for some period of time. If power to the process is interrupted for long enough, it can move significantly away from its desired operating point, and take some time to return once the power is re-applied. When power is reapplied, the reactive gas pressure, target surface coverage, chamber surface coverage, electrical impedance and deposition rate will have changed.

Reproduced with permission of the copyright owner. Further reproduction prohibited without permission.

Although it is clearly important to develop an understanding of these issues, it appears that they have been investigated empirically only.[12] However, to fully realize the potential of reactive sputtering, it will be necessary to systematically develop an understanding based on reliable mathematical models which capture the essential physics of the process. This dissertation addresses the issue by using a model-based approach to determine acceptable maximum power supply arc response shut down times for a representative industrial glass coating process. This is the first time to the author's knowledge that modeling has been used to explore the arc response dynamics of a reactive sputtering process. The methodology and results are presented in Chapter 2.

1.3 Pulsed Reactive Co-sputtering

It is possible to configure a sputtering system such that two different target materials are sputtered, with the power to each of the targets controlled independently, as shown in Figure 1.1.3. This is referred to as co-sputtering. When co-sputtering is performed in the presence of a reactive gas, it is called reactive co-sputtering. The motivation is creation of controlled mixtures of materials in the film deposited by the process. Reactive co-sputtering is appealing because it can deposit films otherwise unrealizable. It allows, for example, the creation of films with customized or graded indexes of refraction. For example, Al_2O_3 can be deposited with a refractive index of about 1.6 and TiO_2 can be deposited with a refractive index of about 2.4. If a co-sputtering arrangement is configured with one Al target and one Ti target, the ratio of Ti to Al can be controlled by controlling the power to each of the magnetrons. Therefore, in principle, it is possible to "dial" the refractive index anywhere between 1.6 and 2.4.

Reproduced with permission of the copyright owner. Further reproduction prohibited without permission.

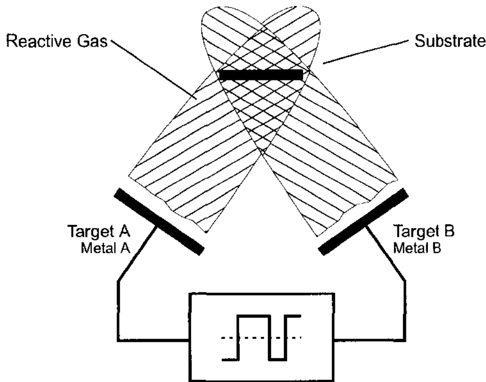

Figure 1.1.3. Pulsed dual magnetron reactive co-sputtering arrangement.

Co-sputtering of two different materials is typically accomplished with ion beam sputtering or the use of RF or DC supplies to deliver power to sputtering targets in diode or magnetron configurations.[13,14] The advent of pulsed supplies which can reliably regulate the power delivered to each magnetron is a key enabling technology for reactive co-sputtering in a conventional dual magnetron sputtering (DMS) arrangement. Pulsed supplies inherently offer more flexibility in control of the process. They provide the capability of independently regulating the power delivered to each magnetron. This has some advantages for existing processes, and enables the implementation of new processes. Independent regulation enables the creation of controlled mixtures of materials in the film when dissimilar materials are used for the magnetron targets. This would allow the creation of films with customized or graded indexes of refraction.

A square wave voltage source supply has been disclosed by Mark.[15] Pulsed voltage source supplies typically demonstrate slow current rise and high peak currents into an arc. Consequently, they have had limited commercial acceptance for dual

Reproduced with permission of the copyright owner. Further reproduction prohibited without permission.

magnetron sputtering applications. Further work has focused on the development of pulsed current source supplies,[16,17,18] with commercial availability of high power pulsed current source supplies at the 120 kW level beginning in early 1998. The first commercial 200 kW unit was shipped in early 2000.[19] Similar supplies at the 20 kW level were available in 1996.[20] Even though pulsed supplies have been available for some time, their use to create films of controlled or graded index of refraction has not been reported to the author's knowledge.

Co-sputtering has typically been reported on a small scale. A constant concern is scaling to large substrates, with sizes appropriate for architectural and automotive glass, as well as large web coaters. Results for large scale inline coaters, using DC power supplies, were reported in 1991.[21,22,23] Several issues of scaling, such as uniformity and film quality, were addressed. However, to the author's knowledge, use of this technique in production has never been reported.

The potential of reactive co-sputtering has motivated several workers to address process models. An early attempt at modeling co-sputtering processes focused on process voltage and current as model outputs.[24] The resulting model was a good beginning, but the algorithms required for model computation were less than transparent. Almost ten years later, an extension of the Berg model was introduced which showed that the basic process curves look qualitatively like those for simple reactive sputtering.[25] Further work has refined the basic approach, but still models equilibrium, and not dynamic, conditions.[26]

A detailed investigation of co-sputtering, based on process modeling, has shown that more than one enabling technology is required. Pulsed dual-magnetron sputtering

Reproduced with permission of the copyright owner. Further reproduction prohibited without permission.

with independent regulation for each magnetron is the required base. However, a closer look shows that both the composition of the film and the deposition rate are in fact functions of the partial pressure of the reactive gas. This result indicates that partial pressure control is also required in order to achieve high quality films of consistent composition.

This dissertation, for the first time known to the author, reports that both independent regulation of power to each magnetron, and reactive gas partial pressure control, are required in order to set both the film composition (hence, index of refraction for an optical film) and deposition rate. This claim is justified by both modeling and experimental data. The experiments were done in a pulsed DMS configuration with partial pressure control, which has not been reported to date to the author's knowledge. The details are presented in Chapter 3 of this dissertation.

1.4 HPPMS Power Supplies for Reactive Sputtering

As the science of vacuum processing has advanced, thin film coating technology has been called on for increasingly difficult tasks. The level of difficulty has been driven largely by advances in semiconductor and data storage technology, motivated by the constant quest for higher density. As characteristic dimensions have decreased and aspect ratios have increased, ionization of the target atoms has become increasingly important. Now, there are applications which work best when a large fraction of the target atoms are ionized, ideally approaching 100%. These applications include semiconductor processing, tribological coatings, and functional coatings, which are often called on for multiple duties. There are multiple advantages of highly ionized target material. Ions can

Reproduced with permission of the copyright owner. Further reproduction prohibited without permission.

be ducted to the work piece by electrical or magnetic fields. This capability has already been exploited for cathodic arc coatings.[27] An electrical bias on the surface of the work piece can cause the ions to go around corners, and cover, or even fill, high aspect ratio features, such as trenches and vias in semiconductor devices.[28,29,30,31] In addition, an electrical bias on the surface of the work piece determines the energy of the ions reaching the surface. These ions can be either target material or process gas. Both types will deliver energy to the surface of the work piece which is controlled by the bias voltage. A properly chosen bias voltage allows for denser, higher quality films, and makes it possible to tune the properties of the film, such as index of refraction, extinction coefficient, conductivity, stress, and density, to match the application.[32,33,34]

In conventional magnetron sputtering, only a tiny fraction of the sputtered target atoms are ionized, on the order of 1%. Plasmas with a large target material ionization fraction have been created by multiple means. Cathodic arc systems can provide high ionization fractions, but at the expense of macro-particles which preclude their use in the many important applications with characteristic dimensions of order 1 micron or smaller, such as semiconductors and hard disk media and heads. The macro-particles can be radically reduced by the use of a magnetic filter, actually a curved duct which transports the target material ions to the work piece over a curved path, but allows macro-particles and neutrals to pass through its walls. The basic cathodic arc technique is now widely used for coating cutting and forming tools with Ti based compounds, such as TiN and $TiAl_xN_y$, and for providing lifetime functional coatings on door hardware and plumbing fixtures. The macro-particles included as part of the process are acceptable for these applications at the present time, but other applications are intolerant of any macro-

Reproduced with permission of the copyright owner. Further reproduction prohibited without permission.

particles, since they are larger than one or more critical dimensions of the work piece or final application.

In the semiconductor manufacturing arena, this problem has been addressed by a combination of conventional sputtering to generate target material atoms, and an inductively coupled plasma to ionize the target atoms.[35]

A new technique has been developed which has the promise of generating highly ionized plasmas with essentially conventional magnetron sputtering vacuum equipment. By providing a pulse with high peak power, roughly two orders of magnitude higher than normally used, it has been possible to achieve high fractions of target material ionization with standard magnetrons.[36,37,38] Target material ionization has been measured experimentally, but the theoretically explanation of the detailed mechanism is still open to the best of the author's knowledge. Reported peak power densities, averaged over the whole target surface area, range from 1 to 3 kW/cm^2, with discharge voltages between 500 and 1000 volts. The high peak powers result in sputtering from the entire target surface, not just the racetrack area, as is common for typical magnetron sputtering. First reported in 1999, this technique has generated a great deal of interest. So far, it has been applied in a research environment to demonstrate the concept for semiconductor via fill and hard tool coatings. This is only just the beginning of the possible applications. This technique is especially promising for reactive sputtering of conductive compounds, such as CrN_x[39] and TiN, for cutting tool and tribological applications. It is expected that fewer macro-particles will be generated by HPPMS than for cathodic arc processes, and that the size of the macro-particles will be significantly smaller. This has already been confirmed in one case where droplet free films of CrN_x were deposited by HPPMS.[39] This is an

Reproduced with permission of the copyright owner. Further reproduction prohibited without permission.

important consideration for emerging dry machining applications, in which no lubricant of any kind is used in the machining process, since they may require higher quality films than those deposited by typical cathodic arc processes today.

The process is postulated to operate in an arc free region,[40] however, it is unlikely to achieve and maintain arc free operation in practical material processing systems. Even sputtering at conventional power levels has significant issues with arcing, and a great deal of effort has gone into developing techniques for the prevention and handling of arcs.[41,42] It has been necessary to detect and actively handle arcs in order to apply sputter deposition to more and more demanding applications. Now arc handling is assumed to be a standard feature, and is in fact a competitive characteristic for commercial sputtering power supplies. It seems necessary to develop pulsed supply technology to both deliver the required peak and average power, and to detect and handle process arcs. Existing successful magnetron pulsing approaches incorporating arc handling are based on fast current rise and inductive energy storage. HPPMS processes operate at low duty factors, on the order of a few percent, and high currents, up to thousands of amperes, where inductive energy storage is inefficient, due to ohmic losses in the inductor and other circuitry, and the voltage drop across the semiconductors in the circuitry. It seems necessary to develop pulsing supplies for HPPMS processes which incorporate arc handling, and which do not incorporate approaches which are fundamentally inefficient for generating high current pulses at low duty factors.

The technology for generating and delivering high peak power pulses was highly developed for driving radars during World War II, and was subsequently declassified and published.[43] It was further developed to serve laser[44,45,46] and high energy physics

Reproduced with permission of the copyright owner. Further reproduction prohibited without permission.

applications.[47,48] In many cases, it was desired to pulse a device to an operating point as quickly as possible and maintain it there for the duration of the pulse. Radar magnetrons are typical of this requirement. In order to operate properly, the pulse must have a specific rate of voltage rise and the flat top portion must be within a certain window. Two key approaches have been used in the past with great success. Two broad categories of pulser technology were developed and reported. The first was the hard tube pulser, in which a vacuum tube switch was used to connect a capacitive energy store to the load at the beginning of the pulse, and then disconnect it to end the pulse. These pulsers were desirable because they offered complete flexibility in pulse format, but were limited in peak power capability and efficiency. Now, this class of pulsers may be called hard switch pulsers, since there are a number of solid state switches which can be used. In fact, high performance solid state modulators have been developed for driving radar magnetrons, using arrays of power metal oxide silicon field effect transistors (MOSFETs) as a switch element, with performance rivaling the best vacuum tube based modulators.[49] As utilization of vacuum tubes for new designs wanes and MOSFET technology moves toward higher current and voltage, it is more and more likely that the job will be done with MOSFETs.

The second broad category was line type pulsers. They incorporated a transmission line, or a lumped element network approximating a transmission line, charged with energy which was discharged into the load. The switches used for the discharge were closing switches, such as thyratrons and spark gaps, which means they had the ability to close, but not to open when current was flowing through them. These pulsers are known for their ability to deliver high peak powers to plasma loads.

Reproduced with permission of the copyright owner. Further reproduction prohibited without permission.

Consequently, they have been widely used in high energy physics and laser applications. However, these applications have often been tolerant of arcing, and in many cases, such the loads themselves were already arcs. The single mesh lumped element pulse forming network, composed of a capacitor and an inductor, has been widely used to pulse laser flash lamps, where delivery of energy and efficiency of implementation are important. However, detection and suppression of arcs is not required, since the lamp discharge is already an arc in normal operation. In contrast, material processing plasmas typically operate in a glow or abnormal glow discharge regime, such that an instability could result in formation of an arc with much higher current density. In that case, it is necessary to detect formation of an arc, and to respond appropriately. The high peak power magnetron sputtering application is a glow or abnormal glow discharge, with plasma confined in the region of the magnetron by crossed electrical and magnetic fields. As such, instabilities can develop in which the large scale discharge collapses into a small arc with high current density. Unhandled, these arcs can begin to preferentially occur in the same location, resulting in damage to both the target surface and the work piece.

The high peak power pulsed magnetron sputtering technique has great promise as a source of highly ionized target atoms. However, without arc handling, the technique is unlikely to succeed commercially. What is required is a pulser capable of high peak power, with the added capability of arc detection and arc handling. In the best case, energy remaining in the discharge circuit would be recycled to the main energy storage elements, and not be dissipated.

The need for arc handling was discerned and a new topology was developed to provide it. A novel topology for this application has been conceptualized, analyzed, and

Reproduced with permission of the copyright owner. Further reproduction prohibited without permission.

realized in hardware. The resulting pulser has been successfully employed to drive sputtering magnetrons to high peak powers at low duty factors. It has also been used to generate novel process results. This effort is described in Chapter 4.

1.5 References

---

[1] R. J. Hill, S. J. Nadel, Coated Glass Applications and Markets (BOC Coating Technology, Fairfield, CA, 1999).
[2] H. J. Gläser, Large Area Glass Coating (Von Ardenne Anlagentechnik, Dresden, 2000).
[3] Brian Chapman, Glow Discharge Processes (Wiley-Interscience, New York, 1980).
[4] W. D. Westwood, Sputter Deposition (AVS, New York, 2003).
[5] S. Schiller et al., Thin Solid Films 72, 475 (1980).
[6] J. Affinito and R. R. Parsons, J. Vac. Sci. Technol. A 2, 1275 (1984).
[7] W. D. Sproul, Thin Solid Films 107, 141 (1983).
[8] W. D. Sproul, J. R. Tomashek, U.S. patent no. 4,428,811, (Jan. 31, 1984).
[9] W. D. Sproul, Surf. and Coatings Technol. 33, 73 (1987).
[10] W. D. Sproul, M. D. Graham, U.S. patent no. 5,942,089, (Aug. 24, 1999).
[11] A. Belkind, A. Freilich, Soc. Vac. Coaters 41st Ann. Tech. Conf. Proc., 321 (1998).
[12] U. Krause, M. Schulze, H. Fuchs, Proc. of the 3rd – ICCG, 173, (2000).
[13] J.-C. Hsu et al., OSA Technical Digest Series 1998, Vol. 9: Optical Interference Coatings, Tucson, AZ, p. 63, (1998).
[14] C. Misiano, E. Simonetti, Vacuum 27, 403 (1977).
[15] G. Mark, US Patent No. 5,303,139, (12 Apr. 1994).
[16] D. Kovalevskii, M. Kishinevsky, US Patent No. 5,777,863, (7 Jul. 1998).
[17] R. A. Scholl, D. J. Christie, US Patent No. 5,917,286, (29 Jun. 1999).
[18] H. Walde et al., US Patent No. 6,005,218, (21 Dec. 1999).
[19] D. J. Christie et al., Proc. of the 3rd – ICCG, 107, (2000).
[20] D. J. Christie, Soc. of Vac. Coaters 39th Annual Tech. Conf. Proc., 320 (1996).
[21] A. Belkind et al., J. Vac. Sci. Technol. A 9, 530, (1991).
[22] A. Belkind et al., Surf. and Coatings Technol. 49, 155, (1991).
[23] R. Laird, A. Belkind, J. Vac. Sci. Technol. A 10, p. 1908, 1992.
[24] K. Steenbeck, E. Steinbeiβ, K.-D. Ufert, Thin Solid Films 92, 371 (1982).
[25] M. Moradi et al., J. Vac. Sci. Technol. A 9, 619 (1991).
[26] S. Berg et al., J. Vac. Sci. Technol. A 16, 1277 (1998).
[27] C. Y. Chan et al., J. Vac. Sci. Technol. A 19, 1606 (2001).
[28] C. A. Nichols, S. M. Rossnagel, S. Hamaguchi, J. Vac. Sci. Technol. B 14, 3270 (1996).
[29] J. Hopwood, Phys. of Plasmas 5, 1624 (1998).
[30] O. R. Monteiro, J. Vac. Sci. Technol. B 17, 1094 (1999).
[31] J. Lu, M. J. Kushner, J. Vac. Sci. Technol. A 19, 2652 (2001).
[32] L. Hultman et al., J. Vac. Sci. Technol. A 9, 434 (1991).
[33] F. Adibi et al., J. Appl. Phys. 73, 8580 (1993).

Reproduced with permission of the copyright owner. Further reproduction prohibited without permission.

[34] P. J. Kelly, R. D. Arnell, J. Vac. Sci. Technol. A 16, 2858 (1998).
[35] S. M. Rossnagel, J. Hopwood, J. Vac. Sci. Technol. B 12, 449 (1994).
[36] V. Kouznetzov et al., Surf. and Coatings Technol. 122, 290 (1999).
[37] K. Macák et al., J. Vac. Sci. Technol. A 18, 1533 (2000).
[38] A. P. Ehiasarian et al., Vacuum 65, 147 (2002).
[39] A. P. Ehiasarian et al., Surf. and Coatings Technol. 163-164, 267 (2003).
[40] V. Kouznetzov, U.S. Patent No. 06,296,742 B1, (2 Oct. 2001).
[41] G. L. Anderson, P. W. Hammond, D. S. Yotive, U.S. patent No. 5,241,152, (31 Aug. 1993).
[42] G. N. Drummond, U.S. patent No. 5,427,669, (27 Jun. 1995).
[43] G. N. Glasoe and J. V. Lebacz, Pulse Generators (McGraw-Hill, New York, 1948).
[44] J. P. Markiewicz, J. L. Emmett, J. Quantum Elec. QE-2, 707 (1966).
[45] D. J. Christie, et al., in 1981 Laser Program Annual Report, UCRL-50021-81, p. 2-54 (Lawrence Livermore National Laboratory, Livermore, 1982).
[46] K. Whitham, D. Larson, B. Merritt, D. Christie, Proc. SPIE – Int. Soc. Opt. Eng. (USA) 735, 12 (1987).
[47] F. B. A. Früngel, High Speed Pulse Technology (Academic Press, New York, 1965).
[48] L. P. Bradley, Pulse power for plasma physics, International IEEE Minicourse notes, Santa Fe, New Mexico, May 20-22, 1981 (unpublished).
[49] D. J. Christie, Microwave Journal, 111 (Jan. 1993).

Reproduced with permission of the copyright owner. Further reproduction prohibited without permission.

CHAPTER 2

REACTIVE SPUTTERING ARC RESPONSE DYNAMICS

2.1 Approach

It is desired to investigate the properties of a representative large scale reactive sputtering process operating in the transition mode between the metallic state (with only a small fraction covered with compound) and the poisoned state (approaching unity coverage with compound) of the target. In particular, the dynamics of the process when the power supply is shut down in response to an unwanted arc are explored. First, a static model is used to find the equilibrium characteristics of the process. Then, a dynamical model is used to study the arc response characteristics of the process. Since the process studied here is operated in the naturally unstable transition region, where the slope of the reactive gas pressure versus flow curve reverses, it must be stabilized with output feedback control to permit successful simulation. Published data are used to construct a model of a representative large area reactive sputtering process, as used in industrial glass coaters. A maximum arc response shutdown time is proposed and is shown to be consistent with available technology.

2.2 Static Model

A static model of the reactive sputtering process has been shown to capture the essential physics of the process at equilibrium. The Berg model,[1] although not the first to

Reproduced with permission of the copyright owner. Further reproduction prohibited without permission.

appear in the literature,[2] is very straightforward, and perhaps the most transparent. This model is based on equilibrium conditions (no dynamics) and simply tracks the reactive gas and the sputtered material to predict deposition rate and partial pressure of the reactive gas. The algorithm has been arranged so that it requires only one pass. That is to say, there is no recursion involved in the calculation of a particular point on the pressure versus flow and rate versus flow curves.

The flow of reactive gas is tracked from the gas inlet to three "consumers" in the process, as shown in Figure 2.2.1. Input flow is Q_{in}, flow to the target is Q_t, flow to the chamber surfaces is Q_s, and flow to the system pump is Q_p. The obvious destination for the gas is the system vacuum pump, but it is also getter-pumped at the target surface and at the chamber surfaces (including the work piece). The flux of the reactive gas to the target and chamber surfaces is F. A simple continuity relationship for gas flow is the result, whereby the input flow is equated to the sum of the flows to the target, chamber, and system pump. Total flow and flows to the pump, target, and chamber surfaces are assumed to be constant.

Reproduced with permission of the copyright owner. Further reproduction prohibited without permission.

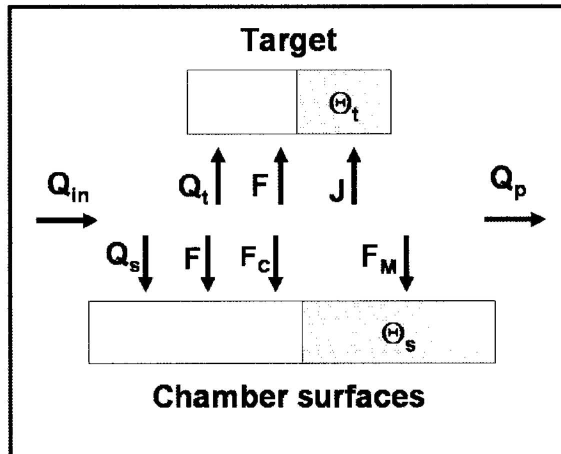

Figure 2.2.1. Reactive sputtering process model diagram.

The next part of the model tracks the fluxes of sputtered material to the chamber surfaces. Material sputtered from the target includes the compound formed at the surface by getter pumping of the reactive gas as well as the intrinsic target material. It is assumed that the flux of material sputtered from the target surface is uniformly directed to the chamber surface, along with the flux of reactive gas. These fluxes are shown schematically in Figure 2.2.1, along with the ion flux directed to the target. The flux of metal from the target is F_M, the flux of compound from the target is F_C, and the sputtering ion current density to the target is J. Perhaps the key concept here is that both the target and the chamber surfaces have covered and uncovered fractions. In this context, the covered fraction is covered with the reactively formed compound. This is important for two reasons. The first is that getter pumping occurs only at the uncovered surfaces, so covering a large fraction of the surface can significantly change the amount of getter pumping that occurs. The second is that the reactively formed compound sputters with a significantly different yield than the target material in many cases.

Reproduced with permission of the copyright owner. Further reproduction prohibited without permission.

At this point, model equations can be discussed. In order to make the model flexible, coefficients are provided to allow specification of the number of gas atoms in the reactive gas molecule and the compound molecule, and specification of the number of metal atoms in the compound molecule.[3]

First, the target coverage fraction is obtained by balancing the formation of compound at the target surface with removal of compound from the target surface by sputtering. Actually, what is equated is the number of reactive gas atoms captured at the surface, and the number of reactive gas atoms in the compound being removed from the surface by sputtering. The rate of reactive gas atom capture, R_{gct} (atoms/sec), at the uncovered fraction of the target surface is

$$R_{gct} = \kappa F(1-\theta_t)A_t\alpha_t \tag{2.1}$$

where κ is the number of atoms in the reactive gas molecule, F (molecules/(m^{2}sec)) is the flux of reactive gas molecules to the target and chamber surfaces, θ_t is the fraction of the target covered with compound, A_t (m^2) is the target area, and α_t is the sticking coefficient of the reactive gas molecules at the bare target material surface. The rate of reactive gas atom removal, R_{grt} (atoms/sec), from the target by sputtering of the compound from the fraction of the target covered with compound is

$$R_{grt} = n_m \frac{J}{q_e}\theta_t A_t S_C \tag{2.2}$$

where n_m is the number of reactive gas atoms in the compound molecule, J (amps/m^2) is the sputtering ion current density at the target surface, q_e $\left(\approx 1.6\times10^{-19}\,\mathrm{C}\right)$ is the elemental charge, and S_C (molecules/ion) is the sputtering yield of the compound. Equating the two

Reproduced with permission of the copyright owner. Further reproduction prohibited without permission.

rates from equations 2.1 and 2.2 yields

$$R_{gct} = \kappa F(1-\theta_t)A_t\alpha_t = n_m \frac{J}{q_e}\theta_t A_t S_C = R_{grt} \tag{2.3}$$

and solving equation 2.3 for the target coverage fraction θ_t results in

$$\Theta_t = \frac{\kappa\alpha_t F}{\kappa\alpha_t F + n_m \frac{J}{q_e} S_C} \ . \tag{2.4}$$

The chamber surfaces coverage fraction θ_s is obtained by balancing the rate of compound formation and deposition on bare metal chamber surfaces with the rate at which compound is covered by metal sputtered from the target. What is actually being equated is the rate of reactive gas atoms, from both the reactive gas flux and compound flux, captured at the bare metal chamber surfaces and the rate of formation of sticking sites for reactive gas atoms by deposition of target material on the chamber surfaces covered with compound. The rate of reactive gas atom capture, R_{gcs} (atoms/sec), at the uncovered fraction of the chamber surfaces is

$$R_{gcs} = \kappa F(1-\theta_s)A_s\alpha_s \tag{2.5}$$

where θ_s is the fraction of the chamber surfaces covered with compound, A_s (m^2) is the chamber surfaces area, and α_s is the sticking coefficient of the reactive gas molecules at the bare metal, or uncovered (by compound) fraction of the chamber surfaces. The rate of reactive gas atoms included in compound molecules deposited on the bare metal fraction of the chamber surfaces, R_{gds} (atoms/sec), incorporating equation 2.2, is

$$R_{gds} = R_{grt}(1-\theta_s) = n_m \frac{J}{q_e}\theta_t A_t S_C(1-\theta_s) \ . \tag{2.6}$$

Reproduced with permission of the copyright owner. Further reproduction prohibited without permission.

The rate of reactive gas atom sticking site creation, R_{gss} (atoms/sec), at the covered fraction of the chamber surfaces is

$$R_{gss} = \frac{n_m}{\beta}\frac{J}{q_e}(1-\theta_t)A_t S_M \theta_s \tag{2.7}$$

where β is the number of metal atoms in the compound, and S_M (atoms/ion) is the sputtering yield of the target material. Equating the rates of reactive gas capture at the chamber surfaces with the rate of reactive gas sticking site creation results in

$$R_{gcs} + R_{gds} = R_{gss} \ . \tag{2.8}$$

Substituting equations 2.5, 2.6, and 2.7 into equation 2.8 and solving for θ_s yields

$$\Theta_s = \frac{\kappa\alpha_s F + n_m\Theta_t \frac{A_t}{A_s}\frac{J}{q_e}S_C}{\kappa\alpha_s F + n_m\Theta_t \frac{A_t}{A_s}\frac{J}{q_e}S_C + \frac{n_m}{\beta}(1-\Theta_t)\frac{A_t}{A_s}\frac{J}{q_e}S_M} \ . \tag{2.9}$$

The flux of the reactive gas molecules to the target and chamber surfaces, assuming a Maxwellian velocity distribution, is

$$F = \frac{P}{\sqrt{2\pi k_b TM}} \tag{2.10}$$

where P (Pa) is the pressure of the reactive gas, k_b $\left(\approx 1.38\times10^{-23}\ \text{J/K}\right)$ is the Boltzman constant, T (K) is the temperature of the reactive gas, and M (kg) is the mass of the reactive gas molecules.

Next, the balance of reactive gas is considered. First, the input flow, Q_{in} (molecules/sec) equated to the consumption by the pumps in the system is

$$Q_{in} = Q_t + Q_s + Q_p \tag{2.11}$$

where Q_t (molecules/sec) is the getter pumping of reactive gas at the target, Q_s

Reproduced with permission of the copyright owner. Further reproduction prohibited without permission.

(molecules/sec) is the getter pumping of the reactive gas at the chamber surfaces, and Q_p (molecules/sec) is the pumping by the system pump. Getter pumping at the target, Q_t, is

$$Q_t = F(1-\Theta_t)A_t\alpha_t \ . \tag{2.12}$$

Getter pumping at the chamber surfaces, Q_s, is

$$Q_s = F(1-\Theta_s)A_s\alpha_s \ . \tag{2.13}$$

Pumping by the system pump, Q_p, is

$$Q_p = S_p\left(10^{-3}\frac{\text{meter}^3}{\text{liter}}\right)\frac{P}{k_bT} \ . \tag{2.14}$$

At this point, there is sufficient definition to relate reactive gas flow to reactive gas pressure. This may be accomplished by choosing a reactive gas pressure, and then evaluating equations 2.10, 2.4, 2.9, 2.12, 2.13, 2.14, and 2.11, in that order, to find the reactive gas flow into the chamber.

Finally, sputtering rate is considered. The total flux of metal atoms to the chamber surfaces, F_R (atoms/(m^{2}sec)), is taken as the rate. It is

$$F_R = \frac{J}{q_e}A_t\left[(1-\Theta_t)S_M + \beta\Theta_tS_C\right]\frac{1}{A_s} \ . \tag{2.15}$$

Sputtering rate may be computed by choosing a reactive gas pressure, then evaluating equations 2.10, 2.4, and 2.15 in that order. Now the equilibrium, or static, relationships between reactive gas pressure, reactive gas flow, and sputtering rate are established.

2.3 Dynamical Model

A dynamical model was used to examine the behavior of the process during an arc response. In particular, behavior of key internal parameters over a short time scale is of

Reproduced with permission of the copyright owner. Further reproduction prohibited without permission.

interest. The model is the dynamical version of the Berg model, configured such that the internal states are partial pressure, target coverage fraction, and chamber surface coverage fraction.[4,5,6]

The dynamical model works by tracking reactive gas atoms at the target surface and chamber surfaces, and in the chamber volume. The number of reactive gas molecules at the target surface, N_t, is

$$N_t = n_m \sigma A_t \theta_t \tag{2.16}$$

where σ (molecules/m^2) is the surface density of the compound molecules. Now the equation relating the time derivative of the number of reactive gas atoms at the target surface to the time derivative of the target coverage fraction is

$$\frac{dN_t}{dt} = n_m \sigma A_t \frac{d\theta_t}{dt} \ . \tag{2.17}$$

The time derivative of the number of reactive gas atoms at the target surface, drawing on equations 2.1 and 2.2, is

$$\frac{dN_t}{dt} = R_{gct} - R_{grt} \ . \tag{2.18}$$

It is possible to relate the time derivative of the target coverage fraction to other system variables. The relationship, which includes compound formation at the target surface by a reaction with the gas flux to the surface and removal of compound from the surface by sputtering can be derived from equations 2.1, 2.2, 2.17, and 2.18. It is

$$n_m \sigma A_t \frac{d\theta_t}{dt} = \frac{dN_t}{dt} = R_{gct} - R_{grt} = \kappa F \alpha_t (1-\theta_t) A_t - n_m \frac{J}{q_e} S_c \theta_t A_t \ . \tag{2.19}$$

The flux of the reactive gas molecules to the surface, assuming a Maxwellian velocity distribution, is defined in equation 2.10. Now, by solving equation 2.19, the time

Reproduced with permission of the copyright owner. Further reproduction prohibited without permission.

derivative of the target coverage fraction is

$$\frac{d\theta_t}{dt} = \frac{1}{n_m \sigma}\left(\kappa F \alpha_t (1-\theta_t) - n_m \frac{J}{q_e} S_c \theta_t \right) . \tag{2.20}$$

Similarly, the model also tracks the number of reactive gas atoms at the chamber surfaces. The equation for the number of reactive gas atoms at the chamber surfaces, N_s is

$$N_s = n_m \sigma A_s \theta_s . \tag{2.21}$$

The equation obtained by taking the time derivative of both sides is

$$\frac{dN_s}{dt} = n_m \sigma A_s \frac{d\theta_s}{dt} . \tag{2.22}$$

The time derivative of the number of reactive gas atoms at the chamber surfaces, drawing on equations 2.5, 2.6, and 2.7, is

$$\frac{dN_s}{dt} = R_{gcs} + R_{gds} - R_{gss} . \tag{2.23}$$

Then the equation relating the time derivative of the coverage fraction to other system variables can be found by substituting equations 2.5, 2.6, and 2.7 into equation 2.23. It is

$$\frac{dN_s}{dt} = \kappa F \alpha_s (1-\theta_s) A_s + n_m F_c (1-\theta_s) A_s - F_M \frac{n_m}{\beta} \theta_s A_s . \tag{2.24}$$

Combining equations 2.22 and 2.24 yields

$$n_m \sigma A_s \frac{d\theta_s}{dt} = \kappa F \alpha_s (1-\theta_s) A_s + n_m F_c (1-\theta_s) A_s - F_M \frac{n_m}{\beta} \theta_s A_s \tag{2.25}$$

where F_c (molecules/(m^{2}sec)) is the flux of compound molecules to the chamber surfaces and F_M (atoms/(m^{2}sec)) is the flux of metal atoms to the chamber surfaces. Solving

Reproduced with permission of the copyright owner. Further reproduction prohibited without permission.

equation 2.25 for the time derivative of the chamber surfaces coverage fraction results in

$$\frac{d\theta_s}{dt} = \frac{1}{n_m\sigma}\left(\kappa F\alpha_s(1-\theta_s) + n_m F_c(1-\theta_s) - F_M\frac{n_m}{\beta}\theta_s\right) . \tag{2.26}$$

The flux of compound molecules to the chamber surfaces from the target is

$$F_c = \frac{J}{q_e}A_t\theta_t S_c\frac{1}{A_s} . \tag{2.27}$$

The flux of metal atoms to the chamber surfaces is

$$F_M = \frac{J}{q_e}A_t(1-\theta_t)S_M\frac{1}{A_s} . \tag{2.28}$$

The next step is to consider the chamber volume equation which relates chamber pressure to flow into the chamber and pumping by gettering and the system pump. Getter pumping is defined by equations 2.12 and 2.13 and pumping by the system pump is defined by equation 2.14. Now, pressure can be related to the number of reactive gas molecules in the chamber by the universal gas law. The equation is

$$P = nk_bT = \frac{N_c}{V_c}k_bT . \tag{2.29}$$

where n (molecules/m^3) is the density of the reactive gas molecules, N_c is the number of reactive gas molecules in the chamber volume, V_c (m^3) is the chamber volume. Solving for N_c yields

$$N_c = \frac{V_c}{k_bT}P . \tag{2.30}$$

Now the time derivative of N_c is the flow into the chamber volume less the flows to the three pumps. The equation is

Reproduced with permission of the copyright owner. Further reproduction prohibited without permission.

$$\frac{V_c}{k_b T}\frac{dP}{dt} = \frac{dN_c}{dt} = Q_{in} - Q_t - Q_s - Q_p \ . \tag{2.31}$$

Solving equation 2.31 for the time derivative of reactive gas pressure yields

$$\frac{dP}{dt} = \frac{k_b T}{V_c}\left(Q_{in} - Q_t - Q_s - Q_p\right) . \tag{2.32}$$

For purposes of this model, the deposition rate is taken as the total flux of metal atoms to the chamber surface, including both atoms from sputtered target material and those atoms included in the compound sputtered from the target surface. The rate,

F_R (atoms/(m^{2}sec)), is

$$F_R = F_M + \beta F_c \ . \tag{2.33}$$

The model lends itself to a state space representation since the dynamics are described by three coupled differential equations. The state vector x is

$$x = \begin{bmatrix} x_1 \\ x_2 \\ x_3 \end{bmatrix} \equiv \begin{bmatrix} P \\ \theta_t \\ \theta_s \end{bmatrix} . \tag{2.34}$$

The input vector is

$$u \equiv [Q_{in}] \ . \tag{2.35}$$

The differential equations describing the coupled dynamics of the three states have already been given in Equations 2.32, 2.20, and 2.26 and the state vector has been defined by Equation 2.34. The system represented as a function of x and u is

$$\dot{x} = f(x,u) \ . \tag{2.36}$$

Now, in order to design a feedback controller for the process, the non-linear system will be linearized[7] so it can be represented as

$$\dot{x} = Ax + Bu \ . \tag{2.37}$$

Reproduced with permission of the copyright owner. Further reproduction prohibited without permission.

where A is a square matrix obtained by taking the Jacobian of $f(x,u)$ with respect to x and evaluating it at the desired operating point, written as

$$A = \frac{\partial}{\partial x} f(x,u) \bigg|_{u = u_{op}, x = x_{op}} . \tag{2.38}$$

where the equilibrium input corresponding to the process operating point is u_{op}, and the state vector at equilibrium is x_{op}. The Jacobian of $f(x,u)$ with respect to u evaluated at the operating point is B, written as

$$B = \frac{\partial}{\partial u} f(x,u) \bigg|_{u = u_{op}, x = x_{op}} . \tag{2.39}$$

The stability of the process at the operating point can be assessed by examining the eigenvalues of A. For stability, the eigenvalues must be in the open left half of the complex plane. If any eigenvalues are in the closed right half of the complex plane, then it will be necessary to stabilize the process model in order to simulate it at the operating point. The stabilization is accomplished by adding feedback to the equilibrium open loop input u_{op}. With state feedback, the input is

$$u = u_{op} + k(x_{op} - x) . \tag{2.40}$$

so the linearized closed loop system matrix, A', becomes

$$A' = A - Bk . \tag{2.41}$$

The stabilizing control design methodology was to use the linear quadratic regulator design technique[8] (LQR) to arrive at a starting place, simply using the identity matrix for both input and state penalties. The result was a state feedback regulator, with feedback from all three states. However, practical means of measuring the coverage fractions do not yet exist, so reactive gas pressure feedback alone was used. This implies that the

Reproduced with permission of the copyright owner. Further reproduction prohibited without permission.

elements of

$$k = [k_1 \quad k_2 \quad k_3] \ . \qquad (2.42)$$

corresponding to the coverage fractions need to be zero, so

$$k_2 = 0 \, , \; k_3 = 0 \, , \text{and } k = [k_1 \quad 0 \quad 0] \ . \qquad (2.43)$$

Closed loop stability must be checked, and the value of k_1 provided by LQR may have to be adjusted to provide sufficient gain margin to simulate the system. This is the first time to the author's knowledge that this technique has been applied to stabilizing feedback controller design for a reactive sputtering process.

2.4 Simulations of Arc Response Dynamics

Simulations were performed with Simulink®.[9] Results of simulations performed using this model highlight the need for rapid arc response, and a managed low arc rate in practical industrial reactive sputtering processes. The results show partial pressure, target coverage fraction, chamber surfaces coverage fraction, and deposition rate as a function of time. Model parameters, listed in Table 2.4.1, were chosen to be representative of a large area, mid-frequency dual magnetron coating process with magnetrons 2 meters long operating at about 120 kW.[10]

Reproduced with permission of the copyright owner. Further reproduction prohibited without permission.

Table 2.4.1. Parameters used for large area TiO_2 process arc response simulation.

Parameter	Value	Comments
Target material	Ti	
Reactive gas	O_2	
Nominal compound	TiO_2	
Surface density of compound molecules	9.7×10^{18} m^{-2}	
Ti sputtering yield	0.5	[10]
TiO_2 sputtering yield	0.017	[10]
Target area	0.264 m^2	
Chamber area	6.06 m^2	
Chamber volume	0.7 m^3	
Pumping speed	7000 l/s	
Temperature	300 K	
Sticking coefficients	1.0	[1]
Oxygen partial pressure	0.1 mTorr	equilibrium
Oxygen flow	570 sccm	equilibrium
Ar ion current density	1060 A/m^2	
Target coverage fraction	0.76	equilibrium
Chamber coverage fraction	0.91	equilibrium

The operating point for simulations in the transition region was calculated by the static model, implemented in an Excel spreadsheet. Results are shown in Figure 2.4.1 and Figure 2.4.2. The transition region is the portion in the curves where the sign of the slope

Reproduced with permission of the copyright owner. Further reproduction prohibited without permission.

is reversed with respect to the beginning and end of the curves. In general, open loop operation in the transition region is impossible, so feedback control must be used to achieve operation there. The transition region operating point chosen for the dynamical simulations is denoted by the black diamonds on the curves.

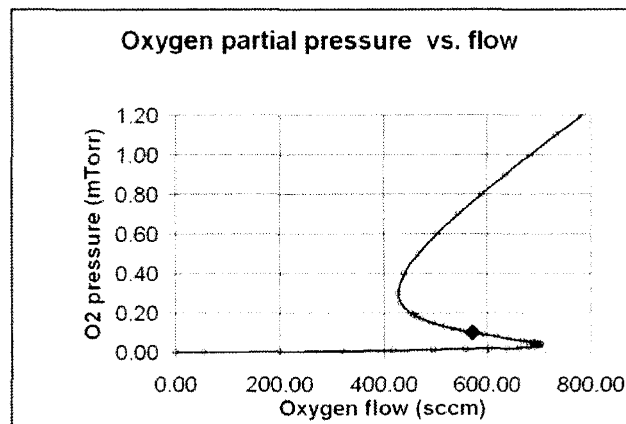

Figure 2.4.1 Oxygen partial pressure versus flow calculations from the static model. The operating point for the dynamical model is denoted by the large diamond on the transition region of the curve.

Reproduced with permission of the copyright owner. Further reproduction prohibited without permission.

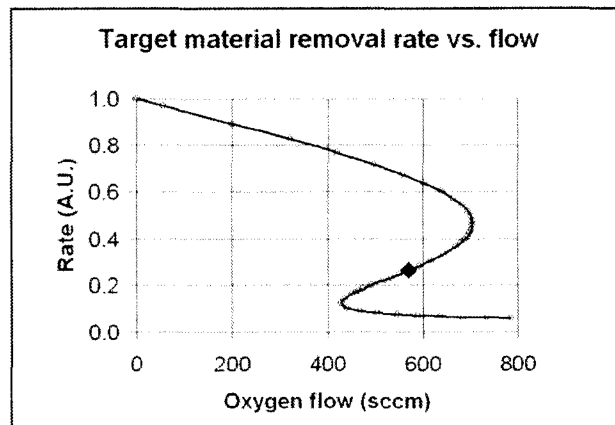

Figure 2.4.2. Deposition rate versus oxygen flow calculations from the static model. The operating point for the dynamical model is denoted by the large diamond on the transition region of the curve.

Response of the process to a 20 msec arc shutdown is shown in Figure 2.4.3. The effect of the shutdown on the deposition rate lasts much longer than the shutdown time, and would likely result in "banding" in an inline glass coater. The drop in rate is much larger than that which might be anticipated by simply looking at partial pressure or target coverage fraction. In fact, a small increase in target coverage fraction can result in a large drop in metal flux to the target because the compound sputters with a much lower yield than the target material. It seems unlikely that this process could be stabilized if shutdowns of this length occurred a few times a second.

Reproduced with permission of the copyright owner. Further reproduction prohibited without permission.

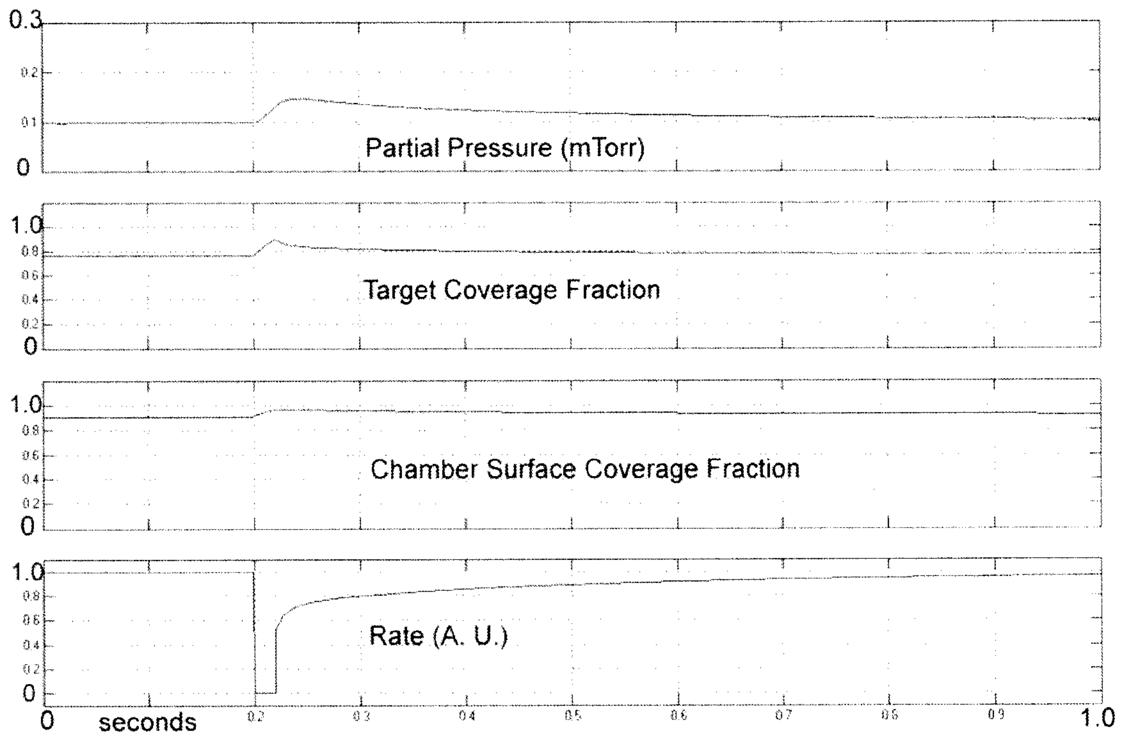

Figure 2.4.3. Process response to 20 msec power supply shutdown in response to an arc.

Figure 2.4.4 shows normalized rate as a function of coverage fraction. Normalized rate, is the effective target material sputtering yield, including both intrinsic target material and target material incorporated in compound at the target surface. The expression for normalized rate, R_{norm}, is

$$R_{norm} = (1-\theta_t)S_M + \beta\theta_t S_C \ . \tag{2.44}$$

Using the concept of normalized rate, equations 2.44 and 2.15 can be combined to get

$$F_R = \frac{J}{q_e} A_t R_{norm} \frac{1}{A_s} \ . \tag{2.45}$$

Reproduced with permission of the copyright owner. Further reproduction prohibited without permission.

So mathematically, R_{norm} is the effective metal sputtering yield for a reactive sputtering process, and is a function of coverage fraction.

Both the equilibrium normalized rate and the normalized rate after a 20 msec shutdown are shown in Figure 2.4.4. The equilibrium coverage fraction is 0.76, with a normalized rate of 0.27. After a 20 msec shutdown, when power is reapplied, the coverage fraction is 0.90, with a normalized rate of 0.13. This explains why just a 20% increase in target coverage fraction can result in a 50% decrease in rate at the time when power is reapplied following an arc response shutdown.

It is also important to note that even if partial pressure could be held absolutely constant, the coverage fraction would increase, with a concomitant decrease in normalized rate.

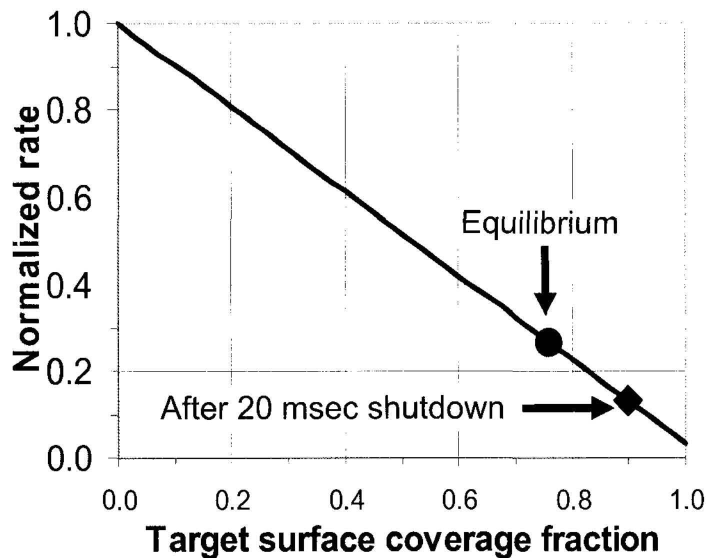

Figure 2.4.4. Normalized rate as a function of coverage fraction for the modeled TiO_2 process.

Reproduced with permission of the copyright owner. Further reproduction prohibited without permission.

A loss of rate may not be the only effect of a long shutdown for arc response. The average target surface coverage fraction also increases, as seen in Figure 2.4.3. This could result in a change of film properties as well. Experimental data for deposition of AlO_x in the transition region shows that the index of refraction decreases from 1.66 to 1.61 as partial pressure is increased, while remaining in the transition region.[11] Equations 2.4 and 2.10 taken together show that as partial pressure is increased, target surface coverage fraction also increases, approaching unity. Therefore, it could be that longer shutdown times will result in films with lower index of refraction, which may indicate a reduction in morphology or density of the films.

Response of the process to a 5.0 msec arc shutdown is shown in Figure 2.4.5. Even a 5 msec shutdown results in a significant disturbance to the process, and it takes some time for the rate to recover to the pre-shutdown level.

Reproduced with permission of the copyright owner. Further reproduction prohibited without permission.

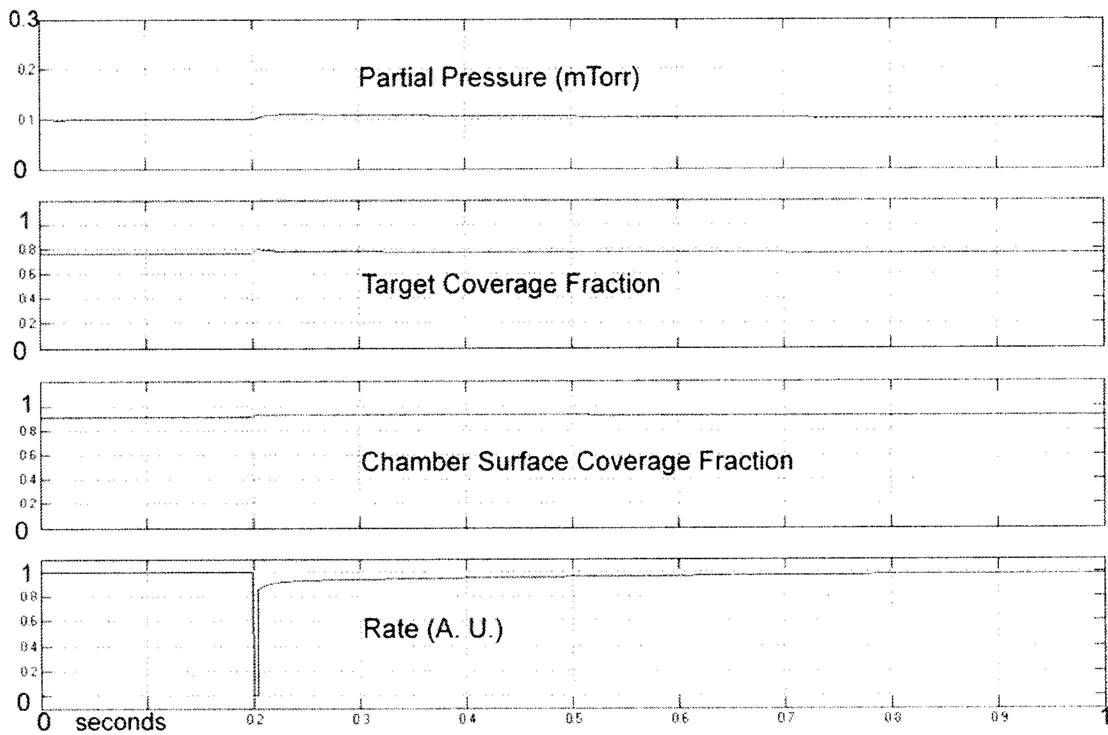

Figure 2.4.5. Process response to 5 msec power supply shutdown in response to an arc.

Response of the process to a 1.0 msec arc response shutdown is shown in Figure 2.4.6. The longer term effect on rate is in the range of a few percent. An arc response shutdown on the order of 1.0 msec or less allows process operation to continue nearly seamlessly after power is restored.

Reproduced with permission of the copyright owner. Further reproduction prohibited without permission.

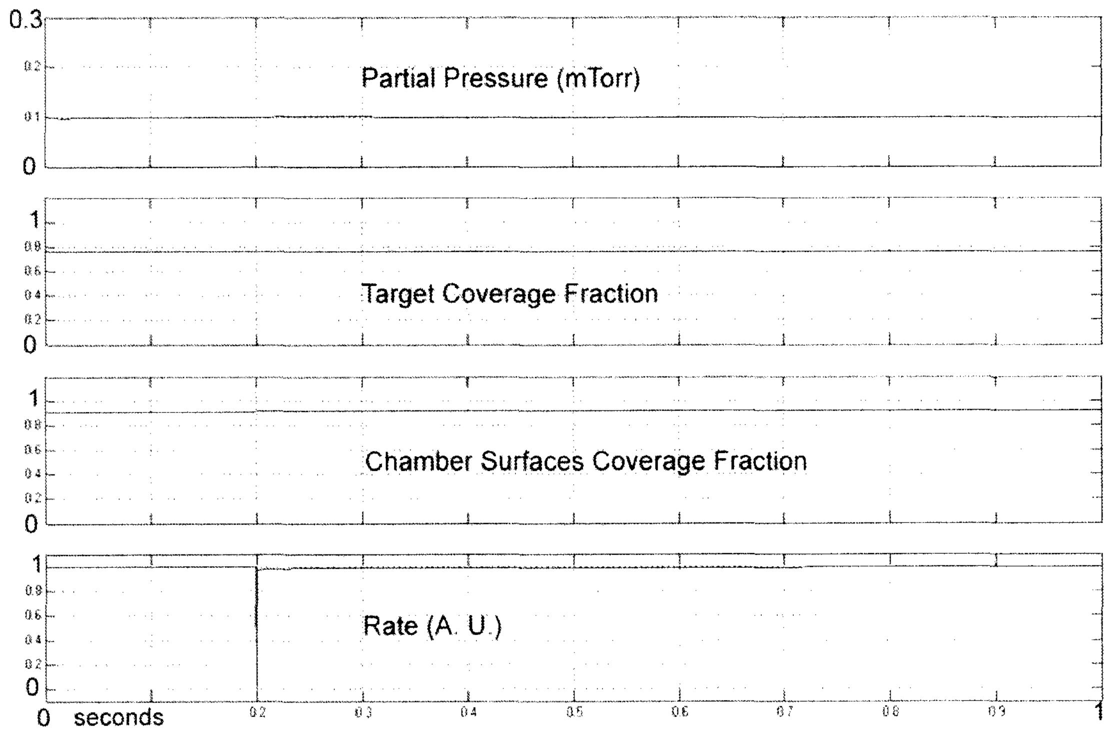

Figure 2.4.6. Process response to 1 msec power supply shutdown in response to an arc.

2.5 Arc Response Requirements

In general, it is desirable to minimize the time the power supply shuts off in response to an arc. It is necessary to shut off long enough to extinguish the arc, but not so long that available deposition rate is wasted.

The simulation results in the previous section showed that a key requirement for stabilization of the deposition rate for processes operating in the transition region is a rapid arc response, less than 1 msec for the system studied. Resonant power supplies optimized for large area dual magnetron sputtering are capable of a complete arc response in less than 1 msec.[12] These power supplies were designed with a low stored

Reproduced with permission of the copyright owner. Further reproduction prohibited without permission.

energy to allow rapid shutoff and re-initiation of high power operation. Arc response from a resonant mid-frequency power supply optimized for plasma processing is shown in Figure 2.5.1 and Figure 2.5.2. Full power operation, at about 150 kW, is restored within 800 μsec after the power supply shuts off to handle an arc.

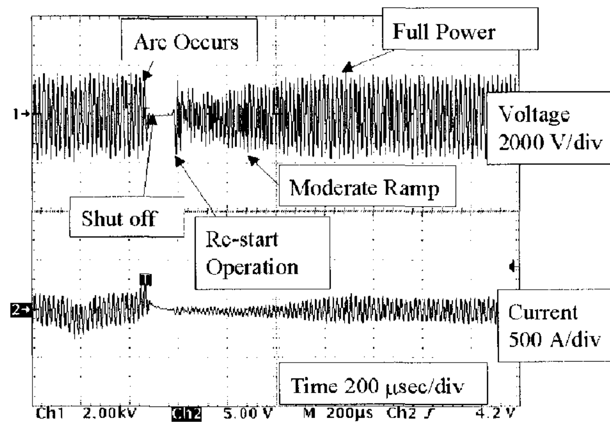

Figure 2.5.1. 180 kW resonant power supply arc response, zoomed out. Full power is restored in 800 μsec.[11]

Reproduced with permission of the copyright owner. Further reproduction prohibited without permission.

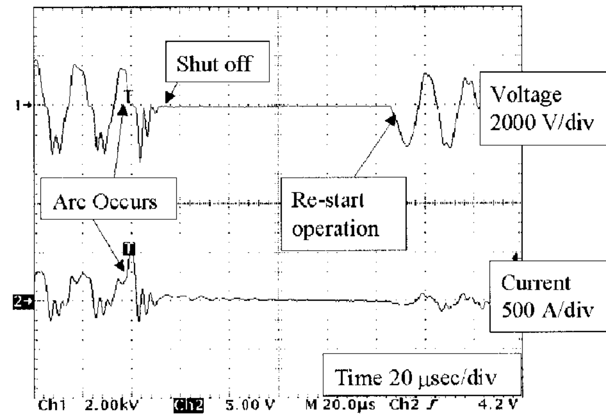

Figure 2.5.2. 180 kW resonant power supply arc response, zoomed in.[11]

Arc response from a mid-frequency dual-magnetron pulsed current source supply is shown in Figure 2.5.3.[13,14,15] Full power is restored in the opposite polarity within about one half-cycle of shutting down to handle an arc. This probably represents about the minimum possible shutdown time for a pulsed dual magnetron reactive sputtering process.

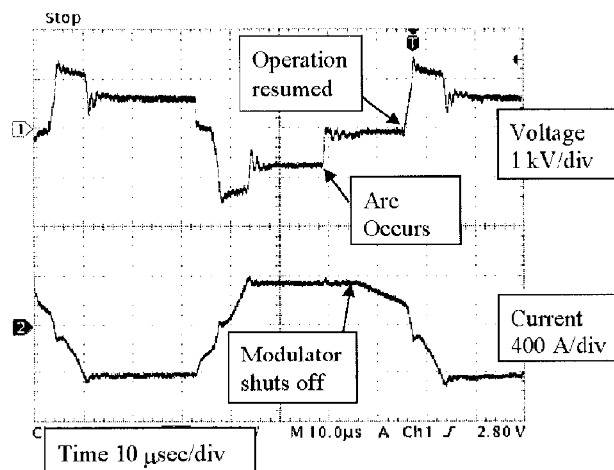

Figure 2.5.3. 200 kW bi-polar pulsed power supply arc response.[12]

Reproduced with permission of the copyright owner. Further reproduction prohibited without permission.

2.6 Summary and Conclusions

Process simulations showed that power supply arc response shutdowns need to be of order 1.0 msec or less to minimize disturbance to the large area transition mode reactive sputtering process studied here. The result of longer shutdown times is a reduction of deposition rate. An additional effect of longer shutdown times may be a change in index of refraction of the films, owing to the increase in average target surface coverage fraction. Experimental data has shown that resonant and pulsed current source supplies optimized for large area mid-frequency dual magnetron sputtering processes can have shutdown times of 800 μsec or less.

2.7 References

[1] S. Berg et al., J. Vac. Sci. Technol. A 5, 202 (1987).
[2] K. Steenbeck, E. Steinbeiβ, K.-D. Ufert, Thin Solid Films 92, 371 (1982).
[3] M. Moradi et al., J. Vac. Sci. Technol. A 9, 619, (1991).
[4] T. Larsson, Vacuum 39, 949, (1989).
[5] N. Malkomes, N. Vergöhl, J. of Appl. Phys. 89, 732 (2001).
[6] H. Bartzsch, P. Frach, Surf. and Coatings Technol. 142-144, 192 (2001).
[7] H. Khalil, Nonlinear Systems (Prentice Hall, Upper Saddle River, 1996).
[8] M. Athans, P. Falb, Optimal Control (McGraw-Hill, New York, 1966).
[9] Using Simulink® (The Mathworks, Natick, 2002).
[10] P. Greene, R. Dannenberg, Soc. Vac. Coaters 42nd Ann. Tech. Conf. Proc., 23 (1999).
[11] W. D. Sproul, B. E. Sylvia, Soc. Vac. Coaters 45th Ann. Tech. Conf. Proc., 11 (2002).
[12] D. J. Christie et al., Soc. of Vac. Coaters 44th Annual Tech. Conf. Proc., 228 (2001).
[13] D. J. Christie et al., Proc. of the 3rd – ICCG, 107, (2000).
[14] R. A. Scholl, D. J. Christie, US Patent No. 5,917,286, (29 June 1999).
[15] R. A. Scholl, D. J. Christie, US Patent No. 6,222,321, (24 April 2001).

Reproduced with permission of the copyright owner. Further reproduction prohibited without permission.

CHAPTER 3

PULSED REACTIVE CO-SPUTTERING

3.1 Approach

The notion of reactive co-sputtering is fundamentally simple. Two different target materials are sputtered in the presence of a single reactive gas, such as oxygen or nitrogen. If either target material is reactively sputtered alone the result is a binary compound, which may be a transparent dielectric film with a distinct index of refraction (the choice of target material and reactive gas to yield a transparent film is assumed here, since the experimental focus of this chapter is on optical films, but is not always the case). These two possible indexes represent the extremes. It seems reasonable to expect that any index between the two extremes could be obtained by varying the relative fraction of each target material. It may also seem that the relative fraction of the target materials in the deposited film could be varied by controlling the power to each target. A process model was used to explore these expectations, and the results were enlightening. Modeling indicated that not only deposition rate, but also relative composition of the film is a strong function of partial pressure, for realistic reactive gas partial pressures in the transition region. This implies the need for reactive gas partial pressure control to successfully deposit high quality films by reactive co-sputtering, particularly in the transition region.

The approach used was to first model the process, and then to confirm model predictions by experiment. The model clearly showed that partial pressure control is

Reproduced with permission of the copyright owner. Further reproduction prohibited without permission.

required in order to stabilize partial pressure and composition of the reactive co-sputtering process. Experiments were performed to confirm this prediction.

3.2 Modeling

The model used was based on one due to Moradi, et al.[1] This model is essentially an extension of the static Berg model.[2] The calculations are performed in a single pass by an Excel spreadsheet. The model shows that important process outputs such as deposition rate and film composition are single-valued functions of the reactive gas partial pressure. However, those process outputs may have multiple values with respect to flow in some process regions.

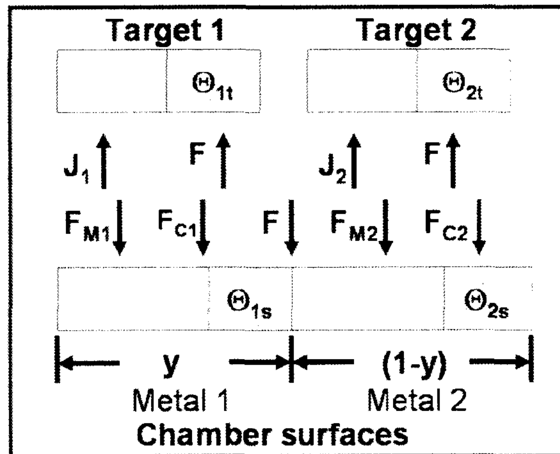

Figure 3.2.1. Reactive co-sputtering model diagram.

The model is shown schematically in Figure 3.2.1. The flux of reactive gas molecules, F (molecules/(m^{2}sec)), to the surfaces of Target 1 and Target 2 and the Chamber Surfaces is

Reproduced with permission of the copyright owner. Further reproduction prohibited without permission.

$$F = \frac{P}{\sqrt{2\pi k_b TM}} \tag{3.1}$$

where P is the pressure of the reactive gas (Pa), T is the reactive gas temperature (K), M is the mass of the reactive gas molecule (kg), and k_b ($\approx 1.38\times10^{-23}$ J/K) is the Boltzman constant. This equation for reactive gas flux assumes a Maxwellian velocity distribution for the reactive gas molecules. It is important to note that the model is based on the molecular reactive gas, although atomic, ionized, excited, and meta-stable states may also present. The basic Berg model has been shown to effectively predict process behavior by utilizing the simplification of considering only reactive gas.[2] Variables J_1 (amp/m^2) and J_2 (amp/m^2) are the sputtering ion current densities at the surfaces of Target 1 and Target 2 respectively. It is important to note that these are the only ion fluxes in the model, even though there would be some natural ion flux from the plasma in the chamber to the chamber walls. The basic Berg model has been shown to effectively predict process behavior by utilizing the simplification of considering only ion flux to the targets for the purpose of sputtering.[2] The fractions of Target 1 and Target 2 covered by the reactive compound are represented by variables Θ_{1t} and Θ_{2t}, respectively. These are the so-called target area coverage fractions, and being fractions, they are dimensionless. The ion flux tends to reduce the target coverage fraction by sputtering the compound molecules away. In contrast, the reactive gas flux tends to increase the coverage fraction by forming more compound molecules on the surface. The sputtering yields are typically quite different for the compound and the target material, with the compound usually having a significantly lower sputtering yield. When everything is considered, there is a unique equilibrium condition for the coverage fractions of the two targets where the rate

Reproduced with permission of the copyright owner. Further reproduction prohibited without permission.

of compound formation equals the rate at which the compound is sputtered away from the surface of the target. The equations for coverage fractions are the result of equating compound formation and compound sputtering rates at the target surfaces. The coverage fraction for Target 1 is

$$\Theta_{1t} = \frac{\kappa \alpha_{t1} F}{\kappa \alpha_{t1} F + n_{M1} \frac{J_1}{q_e} S_{C1}} \tag{3.2}$$

where κ is the number of atoms in the reactive gas molecule, α_{t1} is the sticking coefficient (probability) of the reactive gas molecules to the bare target material, n_{M1} is the number of gas atoms in the compound formed by the reaction between the reactive gas and the material of Target 1, S_{C1} (molecules/ion) is the sputtering yield of the compound consisting of the reactive gas and the material of Target 1, and q_e ($\approx 1.6 \times 10^{-19}$ C) is the elemental charge. Similarly, the coverage fraction for Target 2 is

$$\Theta_{2t} = \frac{\kappa \alpha_{t2} F}{\kappa \alpha_{t2} F + n_{M2} \frac{J_2}{q_e} S_{C2}} \tag{3.3}$$

where α_{t2} is the sticking coefficient (probability) of the reactive gas molecules to the bare material of Target 2, n_{M2} is the number of gas atoms in the compound formed by the reaction between the reactive gas and the material of Target 2, and S_{C2} (molecules/ion) is the sputtering yield of the compound consisting of the reactive gas and the material of Target 2. Equations 3.2 and 3.3 are developed following the same logic as for equation 2.4 in section 2.2. The chamber surfaces are conceptually divided into two sections. The first section is impacted by F_{M1} (atoms/(m^{2}sec)), the sputtered metal flux from Target 1, and F_{C1} (molecules/(m^{2}sec)), the compound molecule flux from Target 1, and the

Reproduced with permission of the copyright owner. Further reproduction prohibited without permission.

reactive gas molecule flux, F. F_{M1} is

$$F_{M1} = \frac{J_1}{q_e} S_{M1}(1-\Theta_{1t})\frac{A_{t1}}{A_s} \tag{3.4}$$

where S_{M1} (atoms/ion) is the sputtering yield of Target 1, A_{t1} (m^2) is the sputtering area of Target 1, and A_s (m^2) is the effective chamber surface area. Similarly, F_{C1} is

$$F_{C1} = \frac{J_1}{q_e} S_{C1}\Theta_{1t}\frac{A_{t1}}{A_s}. \tag{3.5}$$

The fraction of the Chamber Surfaces occupied by Metal 1 and Metal 1 reactive compound is designated by y. The fraction of y occupied by Metal 1 reactive compound is represented by Θ_{1s}. The second section of the Chamber Surfaces, occupied by Metal 2 and Metal 2 reactive compound, is impacted by F_{M2}, the metal flux from Target 2 and F_{C2}, the compound molecule flux from Target 2. F_{M2} is

$$F_{M2} = \frac{J_2}{q_e} S_{M2}(1-\Theta_{2t})\frac{A_{t2}}{A_s} \tag{3.6}$$

where S_{M2} (atoms/ion) is the sputtering yield of Target 2 and A_{t2} (m^2) is the sputtering area of Target 2. F_{C2} is

$$F_{C2} = \frac{J_2}{q_e} S_{C2}\Theta_{2t}\frac{A_{t2}}{A_s}. \tag{3.7}$$

This section is represented by $(1-y)$ and the fraction of it covered by reactive compound is denoted by Θ_{2s}. Assuming unity sticking coefficients for metal atoms and compound molecules on the chamber surfaces, y is

$$y = \frac{(F_{M1} + \beta_1 F_{C1})}{(F_{M1} + \beta_1 F_{C1}) + (F_{M2} + \beta_2 F_{C2})} \tag{3.8}$$

Reproduced with permission of the copyright owner. Further reproduction prohibited without permission.

where β_1 is the number of metal atoms in the compound formed by the reactive gas and target material 1 and β_2 is the number of metal atoms in the compound formed by the reactive gas and target material 2. This equation says that y is the ratio of Metal 1 flux to total (Metal 1 plus Metal 2) metal flux to the chamber surfaces. Now, since y is a fraction of the surface

$$0 \le y \le 1 \Rightarrow 0 \le (1-y) \le 1. \tag{3.9}$$

The notion of a compound molecule flux was introduced as an effective simplification to the model,[3] although it does not capture the exact physics of the process. The model calculates a unique equilibrium for y, Θ_{1S}, and Θ_{2S} based on F, F_{M1}, F_{C1}, F_{M2}, and F_{C2}. The chamber surface coverage fractions are computed by equating the formation and deposition of reactive compound to the covering of compound by the metal flux. Fractions y and $(1-y)$ are treated as being independent of one another. Θ_{1S} is

$$\Theta_{1s} = \frac{\beta_1 \dfrac{\kappa}{n_{m1}} \alpha_{1s} F + \beta_1 F_{C1}}{\beta_1 \dfrac{\kappa}{n_{m1}} \alpha_{1s} F + \beta_1 F_{C1} + F_{M1}}. \tag{3.10}$$

Similarly, Θ_{2S} is

$$\Theta_{2s} = \frac{\beta_2 \dfrac{\kappa}{n_{m2}} \alpha_{2s} F + \beta_2 F_{C2}}{\beta_2 \dfrac{\kappa}{n_{m1}} \alpha_{2s} F + \beta_2 F_{C2} + F_{M2}}. \tag{3.11}$$

Equations 3.10 and 3.11 are developed using the same approach as for equation 2.9 in section 2.2. The final step is to calculate the input reactive gas flow. A continuity equation relates input reactive gas flow to the cumulative consumption mechanisms in the process. These include getter pumping at Target 1, Target 2, and the Chamber Surfaces in

Reproduced with permission of the copyright owner. Further reproduction prohibited without permission.

addition to the reactive gas removed by the system pump. It is assumed that reactive gas molecules impinging on uncovered fractions of the targets or chamber surfaces will react with a probability equal to the relevant sticking coefficient, therefore, it is not necessary to consider stoichiometry of the resulting compound to compute gas consumption by gettering. It is important to recall that the stoichiometry of the compounds is considered in computation of the target and chamber surfaces coverage fractions. The gettering at Target 1, Q_{1t} (molecules/sec), is

$$Q_{1t} = \alpha_{1t} F(1-\Theta_{t1}) A_{t1} \quad . \tag{3.12}$$

The gettering at Target 2, Q_{2t} (molecules/sec), is

$$Q_{2t} = \alpha_{2t} F(1-\Theta_{2t}) A_{t2} \quad . \tag{3.13}$$

The gettering at y, Q_{1s} (molecules/sec), is

$$Q_{1s} = \alpha_{1s} F(1-\Theta_{1s}) y A_s \quad . \tag{3.14}$$

The gettering at $(1-y)$, Q_{2s} (molecules/sec) is

$$Q_{2s} = \alpha_{2s} F(1-\Theta_{2s})(1-y) A_s \quad . \tag{3.15}$$

The pumping by the system pump, Q_p (molecules/sec) is

$$Q_p = S_p \left[10^{-3} \frac{\text{meter}^3}{\text{liter}} \right] \frac{P}{k_b T} \tag{3.16}$$

where S_p (liter/sec) is the pumping speed of the system. The total flow of gas to all of the consumers, Q_{in} (molecules/sec), is

$$Q_{in} = Q_{1t} + Q_{2t} + Q_{1s} + Q_{2s} + Q_p \quad . \tag{3.17}$$

This total gas flow relationship accounts for all of the oxygen consumed in the process, but assumes that it is all molecular, even though the actual process may have atomic

Reproduced with permission of the copyright owner. Further reproduction prohibited without permission.

oxygen as well. The Berg model has been shown to predict the behavior of reactive sputtering processes by making the simplification of assuming that all reactive gas is in molecular form.[2] The total flux of metal atoms from the two targets to the chamber surfaces is

$$R = F_{M1} + \beta_1 F_{C1} + F_{M2} + \beta_2 F_{C2} \tag{3.18}$$

where R is the total flux of metal atoms to the chamber surfaces, including metal incorporated in the fluxes of compounds 1 and 2 from the targets to the chamber surfaces., in (molecules/(m^2sec)). The total flux of metal atoms to the chamber surfaces will be taken as the rate of the process for the model output. The rate will be normalized such that the maximum rate is unity for presentation of the modeling results on the graphs.

The system modeled was Ti and Al, with O_2 as the reactive gas, yielding nominal compounds TiO_2 and Al_2O_3 at the extremes and $TiAl_xO_y$ in the middle. The expected range of possible indexes is approximately 1.66 (Al_2O_3) to 2.4 (TiO_2). Parameters used for the model calculations, with references and comments where appropriate, are listed in Table 2.2.1. Sticking coefficients were all assumed to be unity, as has been customary in several papers on modeling reactive sputtering and co-sputtering to date.[1,2,3] This model requires an effective sticking coefficient. Although there has been work done on sticking coefficients for chemisorption,[4] coefficients relevant to the Berg model are not available to the best of the author's knowledge. The reactive gas was assumed to be all molecular, as discussed earlier. The model was configured to provide graphs of rate versus flow, flow versus pressure, composition versus pressure, and rate versus pressure.

Reproduced with permission of the copyright owner. Further reproduction prohibited without permission.

Table 3.2.1. Reactive co-sputtering model parameters.

Parameter	Symbol	Value	Comments
Ti sputtering yield	S_{M1}	0.5	[3]
TiO_2 sputtering yield	S_{C1}	0.017	[3]
Al sputtering yield	S_{M2}	0.8	[5]
Al_2O_3 sputtering yield	S_{C2}	0.025	[4]
Sticking coefficients (all)	α_{xy}	1	[1,2,3]
Ti target area	A_{t1}	0.068 m^2	Estimated
Al target area	A_{t2}	0.068 m^2	Estimated
Chamber area	A_s	1.46 m^2	Estimated
Ti target current density	J_1	294 A/m^2	1 kW, 500 V
Al target current density	J_2	367 A/m^2	1 kW, 400 V
Pumping speed	S_p	465 l/sec	Measured
Gas	n/a	O_2	Known
Temperature	T	300 K	Estimated

Figure 3.2.2 shows the rate versus flow curve. Even though there are two targets with two metals, there is only a single s-curve, similar to the classic s-curve for reactive sputtering with one target material. This suggests that the process could behave similarly to a standard reactive sputtering process, and shows that simple flow control will not allow access to the part of the process space with a positive slope, since there are places on the curve where a single value of flow has three possible values of O_2 partial pressure.

Reproduced with permission of the copyright owner. Further reproduction prohibited without permission.

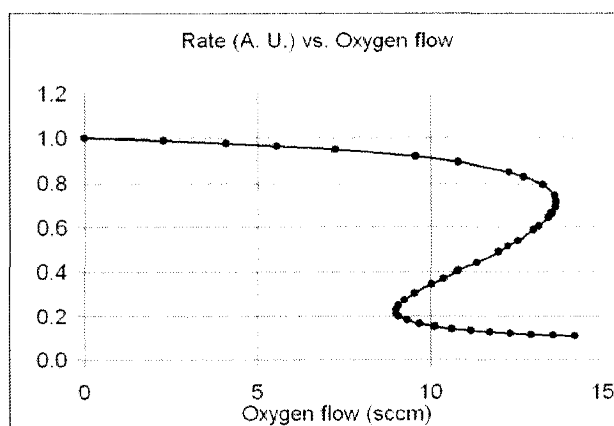

Figure 3.2.2. Model calculation of rate versus flow.

Figure 3.2.3 shows the flow versus pressure curve which accompanies Figure 3.2.2. The transition region is the portion of the curve between the local maximum of flow which occurs at about 0.01 mTorr to local minimum which occurs at about 0.09 mTorr. Flow decreases monotonically with pressure in this portion of the curve, suggesting the application of partial pressure control. The transition region could also be described as the portion of the curve where the derivative of flow with respect to partial pressure is negative.

Reproduced with permission of the copyright owner. Further reproduction prohibited without permission.

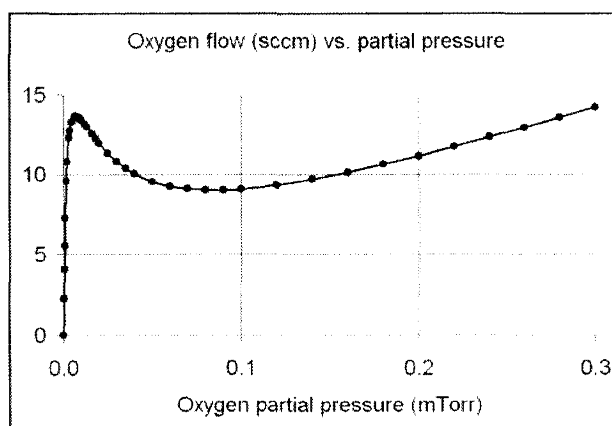

Figure 3.2.3. Model calculation of oxygen flow versus oxygen partial pressure.

Figure 3.2.4 shows the Ti fraction of the metal atoms in the film. This fraction would correlate to index of refraction. It is a strong function of partial pressure in the transition region, and is relatively constant in the poisoned region, greater than about 0.08 mTorr.

Reproduced with permission of the copyright owner. Further reproduction prohibited without permission.

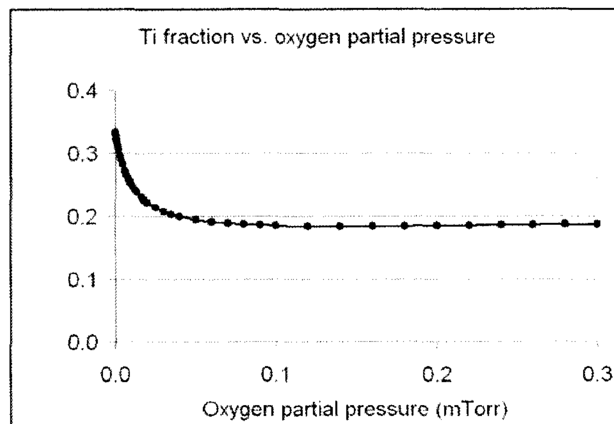

Figure 3.2.4. Model calculation of film composition (fraction of metal that is Ti) versus oxygen partial pressure.

Figure 3.2.5 shows the rate in arbitrary units (A.U.). This is actually calculated as the rate at which metal atoms are removed from the two targets, including the metal in the compound sputtered from the targets. Rate decreases strongly with pressure in the transition region. However, rate continues to decrease significantly with pressure in the poisoned region, where composition is relatively constant. This suggests the desirability of partial pressure control for stabilization of the deposition rate.

Reproduced with permission of the copyright owner. Further reproduction prohibited without permission.

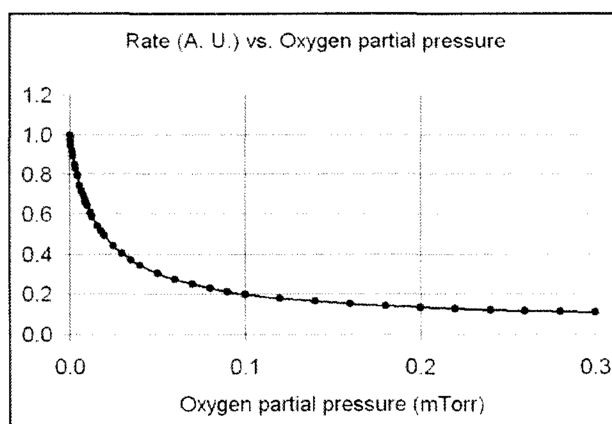

Figure 3.2.5. Model calculation of rate versus oxygen partial pressure.

3.3 Experimental conditions

Data were generated in a medium sized, open-volume, general purpose cylindrical vacuum chamber (about 0.75 m diameter x 0.45 m deep) with a generous number of flanges, of different sizes, style and orientation. The chamber was equipped with two 0.15 m Kurt Lesker Torus 10 balanced-field magnetrons. Distribution of the reactive gas was achieved using simple diffusers. The chamber was turbo-molecular pumped to base pressures below 5×10^{-6} Torr prior to deposition runs. Aluminum and titanium targets were sputtered using an Advanced Energy® Astral™ 20kW pulsed-dc power supply system,[6] capable of independently regulating power delivered to each magnetron. Reactive gas partial pressure was controlled by an IRESS gas control system.[7] This system was developed by Reactive Sputtering Incorporated (RSI). RSI has subsequently been acquired by Advanced Energy®. This system uses an Inficon Transpector® mass spectrometer to measure the relative partial pressures of the reactive gas and the Argon also used for sputtering. Total pressure is measured by a capacitance manometer or

Reproduced with permission of the copyright owner. Further reproduction prohibited without permission.

similar device, such as a Baratron® manufactured by MKS. The inlet of the reactive gas to the chamber is accomplished with a fast piezoelectric valve mounted close to the chamber. A simple manifold is used to distribute the gas inside the chamber to the two magnetrons and the sample being coated. A sample holder capable of holding eight 3 inch by 1 inch glass microscope slides was mounted at 45 degrees to the normal of each magnetron surface. The sample holder incorporates a shutter, to allow the process to run prior to deposition. It also incorporates the ability to change samples under vacuum, allowing eight distinct deposition experiments per chamber pump cycle.

Film thicknesses were measured on glass substrates using a Tencor P200 profilometer and a Gaertner L116 ellipsometer. Index of refraction was measured on a Gaertner L116 ellipsometer. Deposition system parameters are listed in Table 3.3.1

Table 3.3.1. Experimental deposition system parameters.

Parameter	Value	Comments
Ar flow	50 sccm	
Ar pressure	≈ 1.5 mTorr	
Substrate angle	45 deg	To Ti and Al target surface normals
Ti target to Al target angle	90 deg	Angle between surface normals
Ti target to sample distance	0.254 m	
Al target to sample distance	0.185 m	
Pulse frequency	50 kHz	
Duty Cycle	50 %	

Reproduced with permission of the copyright owner. Further reproduction prohibited without permission.

3.4 Results and Discussion

Transparent films with indexes of refraction from about 1.7 to 2.3 were deposited in the course of the experimental campaign, indicating a wide range of compositions.

Oxygen flow versus oxygen partial pressure data were taken at a number of power balance points between the Al and the Ti targets. The total power was kept at 2000 watts. Results are shown in Figure 3.4.1. These curves are similar in character to the curve in Figure 3.2.3, which was generated by the model. In particular, they are monotonic in the transition region, as described in Section 3.2. This allowed use of partial pressure regulation to maintain operation at a fixed transition region set point at all of the power balances investigated experimentally. In fact, partial pressure regulation was used to maintain operation at every point on the curves, representing about 100 experimental data points.

The rate and composition experiments proved difficult to conduct, and machine time was limited. Consequently, experiments were chosen to show the existence of sensitivity of both rate and composition (index of refraction) to the partial pressure of oxygen. Figure 3.4.2 and Figure 3.4.3 show experimental results with both targets in power control mode. The data points plotted correspond to 7 process runs. The Ti target was operated at 1333 W and the Al target was operated at 667 W for a total of 2000 W. Partial pressure was measured with the mass spectrometer and regulated by the IRESS system. In Figure 3.4.2, the rate shows a significant sensitivity to partial pressure, while Figure 3.4.3 shows that the index of refraction is relatively insensitive to the same change in partial pressure. This could be consistent with operation in or close to the poisoned region.

Reproduced with permission of the copyright owner. Further reproduction prohibited without permission.

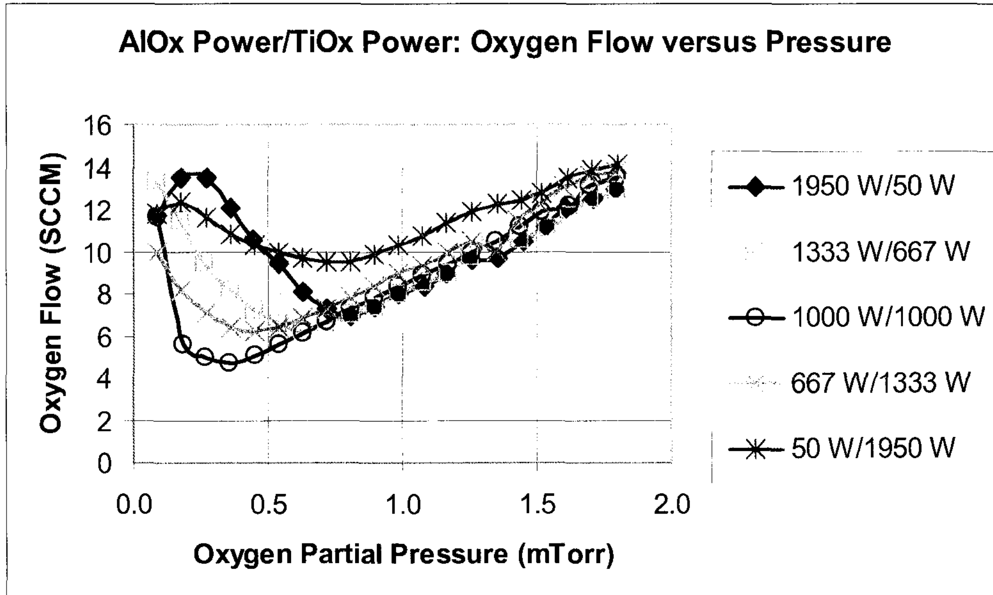

Figure 3.4.1. Experimental flow versus pressure curves for a range of power balances between the Al and Ti targets.

Reproduced with permission of the copyright owner. Further reproduction prohibited without permission.

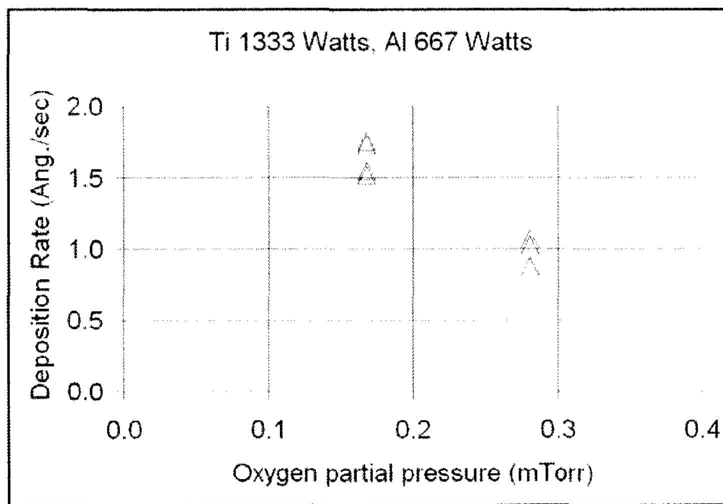

Figure 3.4.2. Experimental deposition rate versus oxygen partial pressure data (Ti 1333 Watts, Al 667 Watts).

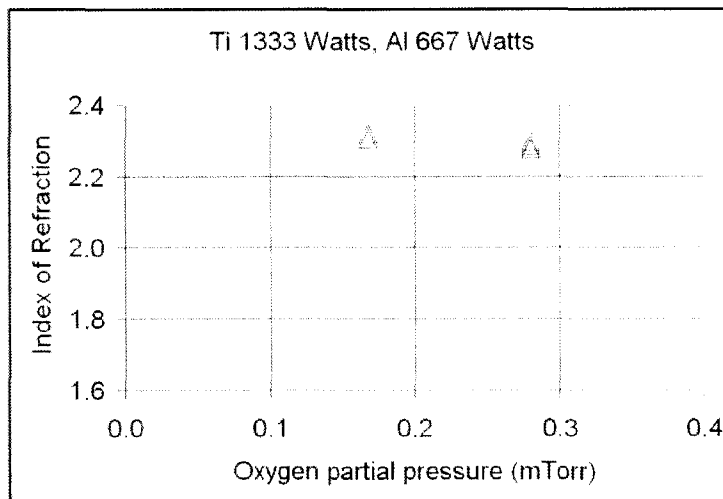

Figure 3.4.3. Experimental index of refraction versus oxygen partial pressure data (Ti 1333 Watts, Al 667 Watts).

Reproduced with permission of the copyright owner. Further reproduction prohibited without permission.

Figure 3.4.4 and Figure 3.4.5 show experimental results with both the Ti and the Al targets operated at 1000 W, for a total of 2000 W. The data points plotted in these figures represent results from seven samples. Figure 3.4.4 shows that rate is relatively insensitive to the change in partial pressure from about 0.17 to 0.28 mTorr, although the rate changes slightly, while Figure 3.4.5 shows that index is sensitive to the same change in pressure. This suggests that the partial pressure is in a range where composition and rate are both changing, which could be the transition region.

These experiments show the existence of sensitivity of both rate and composition (index) to partial pressure. They also support the notion that partial pressure regulation and independent power regulation are required in order to gain control over rate and composition (index) in pulsed reactive co-sputtering processes.

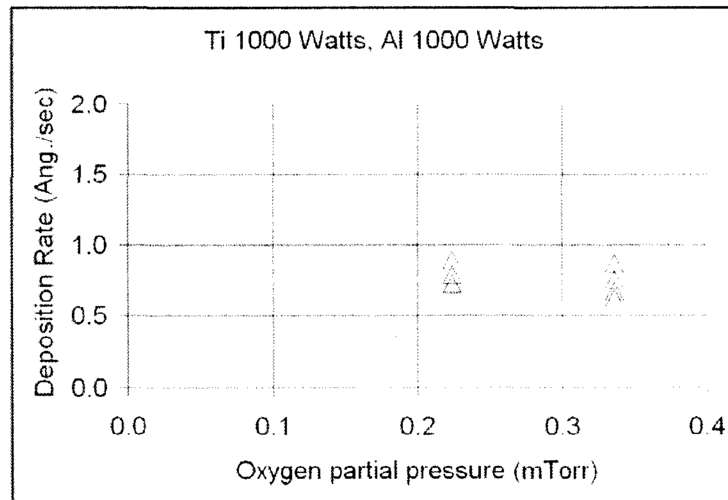

Figure 3.4.4. Experimental deposition rate versus oxygen partial pressure data (Ti 1000 Watts, Al 1000 Watts).

Reproduced with permission of the copyright owner. Further reproduction prohibited without permission.

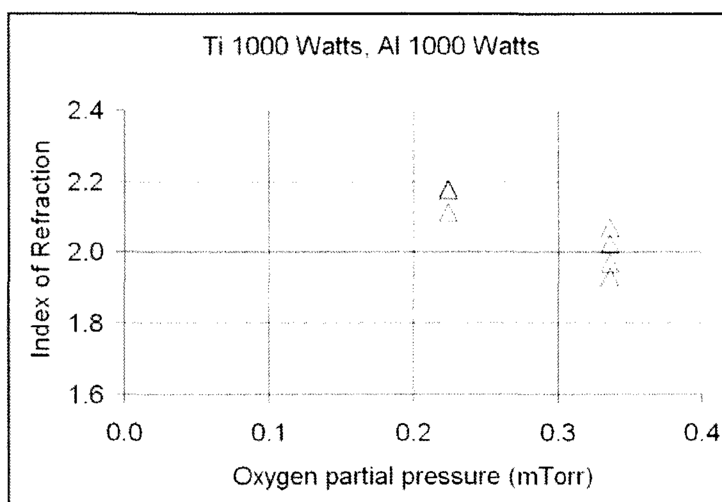

Figure 3.4.5. Experimental index of refraction versus oxygen partial pressure data (Ti 1000 Watts, Al 1000 Watts).

3.5 Conclusions

Mid-frequency dual magnetron co-sputtering can be used to produce optical thin films with customized index of refraction. Modeling has been used to gain insight into the process. Films with indexes from about 1.7 to 2.3 have been deposited using Ti and Al targets, with O_2 for the reactive gas. Refractive indexes in this range are useful for optical coatings. Existence of sensitivity of both rate and composition (index) to partial pressure has been demonstrated experimentally. Pulsed current source power supplies provide independent power regulation for each magnetron. Reactive gas partial pressure controllers allow stable operation in the transition region, and stabilization of rate and index. Both are enabling technologies for mid-frequency dual magnetron reactive co-sputtering.

Reproduced with permission of the copyright owner. Further reproduction prohibited without permission.

3.6 References

[1] M. Moradi et al., J. Vac. Sci. Technol. A 9, 619, (1991).
[2] S. Berg et al., J. Vac. Sci. Technol. A 5, 202 (1987).
[3] P. Greene, R. Dannenberg, Soc. Vac. Coaters 42nd Ann. Tech. Conf. Proc., 23 (1999).
[4] J. B. Hudson in Foundations of Vacuum Science and Technology, Ed. J. M. Lafferty, (Wiley-Interscience, New York, 1998).
[5] L. Jonsson, T. Nyberg, S. Berg, J. Vac. Sci. Technol. A 18, 503, (2000).
[6] Astral Accessory, Advanced Energy product data sheet, (2000).
[7] W. D. Sproul, B. E. Sylvia, Vac. Technol. and Coating, 33 (Aug. 2001).

Reproduced with permission of the copyright owner. Further reproduction prohibited without permission.

CHAPTER 4

POWER SUPPLIES FOR HIGH POWER PULSED REACTIVE SPUTTERING

4.1 Approach

The technology of high power pulsed magnetron sputtering (HPPMS) is considered here. The approach taken is to first work through the basic theory of designing capacitor discharge circuits for plasma loads. A methodology is developed to show by simulation that these designs can be relatively insensitive to the exponent, x, when

$$i \propto v^x \tag{4.1}$$

where i (amperes) is current and v (volts) is voltage. Next, modifications to the basic single mesh pulse forming network to enable process arc handling are considered, resulting in a novel topology which adds arc handling with inductor energy recycling to the basic discharge circuit. Operation of the proposed circuit is verified by simulation and experiment.

An experimental pulser capable of arc detection and handling was constructed and its performance was verified on two magnetron plasma loads, one large (0.30 m by 1.12 m) and one small (0.15 m diameter). Following initial testing, the pulser was used in collaborative research efforts where it demonstrated that the addition of arc handling to an HPPMS power supply can enable interesting new thin film deposition processes. In particular, the pulsed supply was used to deposit dense (2.7 g/cm^3) thin (< 200 Å) carbon films,[1] and reactive deposition of dielectric films on dielectric substrates.[2]

Reproduced with permission of the copyright owner. Further reproduction prohibited without permission.

4.2 Discharge Circuit Design Considerations

What is desirable is a pulse forming approach whose peak output current can be set by capacitor charge voltage when driving a plasma load, and whose current rate of rise and peak output current are limited in the event of an arc. A resonant network, which in its simplest manifestation is composed of a capacitor and an inductor, can provide these characteristics. The basic discharge circuit, the single mesh pulse forming network (PFN), is shown in Figure 4.2.1.

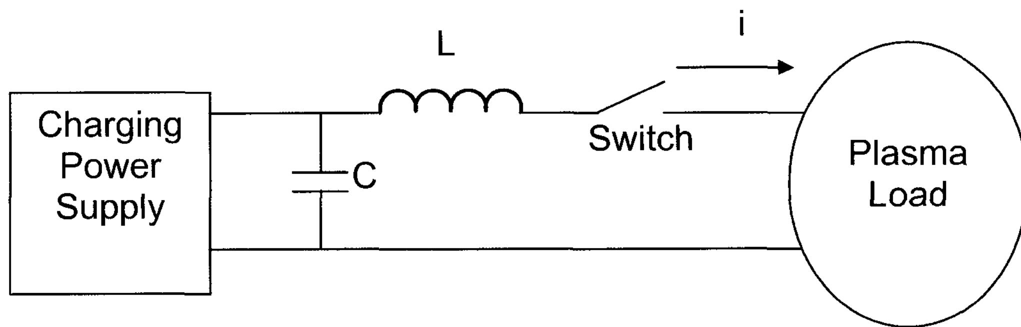

Figure 4.2.l. Basic inductor/capacitor discharge circuit.

The characteristic impedance, Z_0 (ohms), of the resonant network is

$$Z_0 = \sqrt{\frac{L}{C}} \tag{4.2}$$

where C is capacitance (farads) and L is inductance (henrys).[3] The characteristic impedance has the interesting function of relating the capacitor charge voltage, V_{chg} (volts), and the peak current, I_{peak} (amperes), when the load is a short circuit, or, zero

Reproduced with permission of the copyright owner. Further reproduction prohibited without permission.

ohms. The mathematical relationship in that case is

$$I_{peak} = \frac{V_{chg}}{Z_0} \ . \tag{4.3}$$

When discharged into a plasma load, the peak current is somewhat more difficult to predict. The discharge circuit must be designed considering the characteristics of the load. Material processing plasma loads typically exhibit current which is non-linear with respect to voltage and may also have dynamical characteristics which must be considered in the design of the discharge circuit. For the initial design, it may be possible to neglect dynamical characteristics and focus on the load line of the plasma. It is difficult to know *a priori* what the exact characteristics of the load will be. However, it may be possible to estimate or postulate a peak power, and perhaps estimate voltage and current at the peak power condition. This suggests a concept of large signal impedance, based on the voltage and current at the peak power condition. A resistive load condition can be considered to gain some initial intuition regarding the characteristics of the discharge circuit. The simplest approach is to design the PFN to drive a resistive load having the same value as the large signal impedance. The matched load condition for the plasma is chosen such that the peak current is half the short circuit current. If the load were resistive, it would have a resistance R_{load} (ohms) of

$$R_{load} = Z_0 \ . \tag{4.4}$$

For a resistive load, the peak output current may be approximated as

$$I_{peak} \approx \frac{V_{chg}}{(Z_0 + R_{load})} \ . \tag{4.5}$$

Now, to gain some intuition about how things might work for a plasma load the load

Reproduced with permission of the copyright owner. Further reproduction prohibited without permission.

voltage, V_{plasma} (volts), can be assumed to be constant. This was actually close to reality for HPPMS experiments with carbon once the discharge was established.[1] In that case, the load voltage, V_{plasma}, is subtracted from the charge voltage, V_{chg}, and the peak output current is estimated as

$$I_{peak} \approx \frac{(V_{chg} - V_{plasma})}{Z_0} . \tag{4.6}$$

In all cases, it is clear that the characteristic impedance of the network has a large influence on the peak current. In fact, it provides a ballast, and sets an upper limit on the output current. It is due to these characteristics that this circuit has been so widely used to drive flash lamps for photographic, stroboscopic, laser, and photo-reproductive applications.

It is necessary to design the PFN with several key parameters in mind. The PFN must be designed for a specific pulse width and load impedance.

The width of the pulse, t_w (sec), may be estimated as

$$t_w \approx 3\sqrt{LC} . \tag{4.7}$$

One design approach is to fix the pulse width and calculate capacitance and inductance required for a range of characteristic impedances. As an example, Figure 4.2.2 shows the calculated capacitance and inductance for a nominal 100 μsec pulse width for characteristic impedances from 0.5 ohms to 3.0 ohms.

Reproduced with permission of the copyright owner. Further reproduction prohibited without permission.

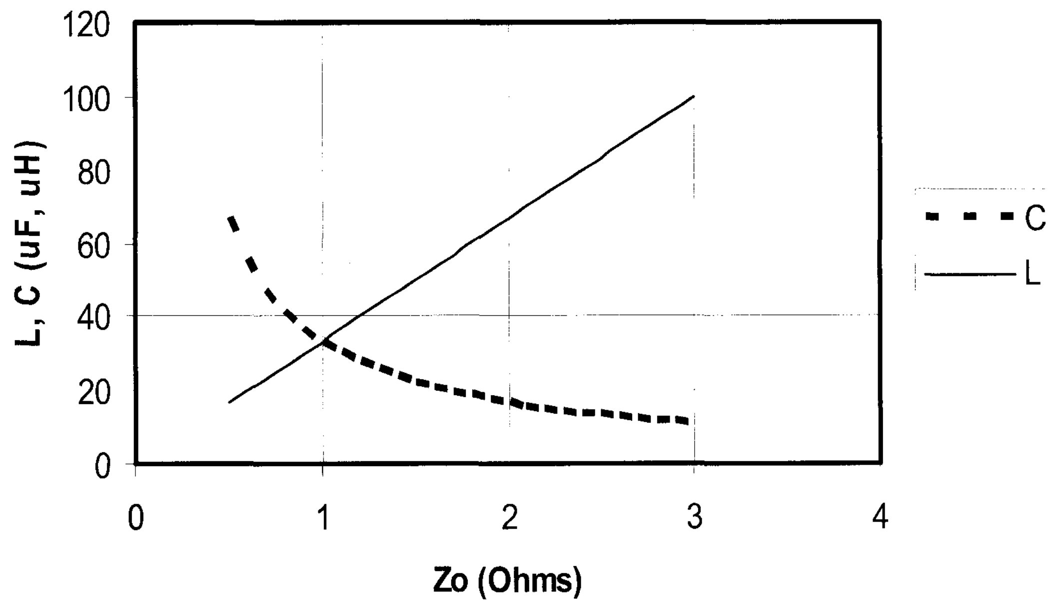

Figure 4.2.2. Capacitance (C) and inductance (L) selection for various characteristic impedances (Z_0) and a fixed 100 μsec pulse width.

One of the key considerations for the design of the pulsing circuit is current rate of rise into a short circuit. Switches for high currents and high peak power have limitations to their operational parameter space. One limitation is the current rate of rise when the switch is turning on. Another is the maximum current the switch can interrupt. In the event of operation into a short circuit, or an arc, the current will increase rapidly. If the rate of rise is not controlled, or managed, then the current may increase beyond the point where the switch is able to open without failing. When discharged into a short circuit, the resonant circuit will exhibit sinusoidal ringing with a frequency, f_0 (Hz), equal to

Reproduced with permission of the copyright owner. Further reproduction prohibited without permission.

$$f_0 = \frac{1}{2\pi\sqrt{LC}} \quad . \tag{4.8}$$

With no damping, operating into a short circuit, the current, i (amperes) is

$$i = \frac{V_{chg}}{Z_0} \sin\left(\frac{t}{\sqrt{LC}}\right) \tag{4.9}$$

where t (sec) is time.

Operation into a short circuit results in the largest possible current rate of rise, which is

$$\text{maximum}\left(\frac{\mathrm{d}i}{\mathrm{d}t}\right) = \frac{V_{chg}}{Z_0\sqrt{LC}} = \frac{V_{chg}}{L} \tag{4.10}$$

by substituting equation 4.2 for Z_0. This is the largest possible magnitude of the rate of rise for any condition with a resistive, plasma, short circuit, or arcing load.

The simple single mesh PFN, composed of an inductor and capacitor in series, has the ability to limit peak current and current rate of rise. It is also tolerant of additional inductance (from output cables, for example) in series with the load, since the circuit already has inductance in series with the output. So, for a typical pulse, the simple single mesh PFN discussed in this section will be suitable. However, without additional circuitry, it will be unable to effectively handle an arc in the plasma processing load. Arc handling requires that the power source be disconnected from the load to limit arc energy and arc related damage to the target and workpiece, and to extinguish the arc.

There are a range of design approaches possible for synthesis of pulse forming network capacitance and inductance values. This problem has been considered in some detail for laser flash lamp PFNs.[4] In this case, it was assumed that current is proportional to voltage squared and a family of normalized solutions useful for flash lamp drive circuit design was obtained.

Reproduced with permission of the copyright owner. Further reproduction prohibited without permission.

With HPPMS magnetron plasma loads, it is nearly impossible to quantify the voltage current characteristics with a simple analytical expression. Simply designing for the characteristic impedance of the network to match the large signal impedance of the plasma load at the peak current is perhaps the most straightforward. At this point, the validity of this simple approach will be examined.

It has been fairly common to view the plasma load current as proportional to an exponential function of voltage, at least in a limited region of the operating parameter space. In that case, the current i_{load} (amperes) would be expressed as

$$i_{load} = \psi v_{load}^{\ x} \qquad (4.11)$$

where ψ (amperes/volt^x) is the proportionality constant, v_{load} is the voltage at the plasma load, and x is the exponent to which the load voltage is raised. Next an illustrative example will be considered. In this case, the desired peak current is 300 A, at a load voltage of 760 V, yielding a large signal impedance of 2.53 Ω. A range of exponents from 0.5 to 4.0 will be considered to examine the validity of a simple analytical design synthesis approach. This range is representative of reported data for HPPMS sputtering of Cu, Cr, and Al.[1,5,6] The values of x and ψ are considered are listed in Table 4.2.1. Values of ψ are computed by solving equation 4.11 for ψ and using voltage and current values for the desired operating point and the desired exponent, x. The voltage – current (VI) characteristics for these four cases are plotted in Figure 4.2.3. The curves all cross at the desired operating point, since x and ψ were chosen such that each curve would pass through the desired operating point.

Reproduced with permission of the copyright owner. Further reproduction prohibited without permission.

Table 4.2.1. Example exponent and proportionality constant values.

x	ψ
0.5	$1.09\times10^{+01}$ amperes/volt$^{0.5}$
1.0	3.95×10^{-01} amperes/volt$^{1.0}$
2.0	5.19×10^{-04} amperes/volt$^{2.0}$
4.0	8.99×10^{-10} amperes/volt$^{4.0}$

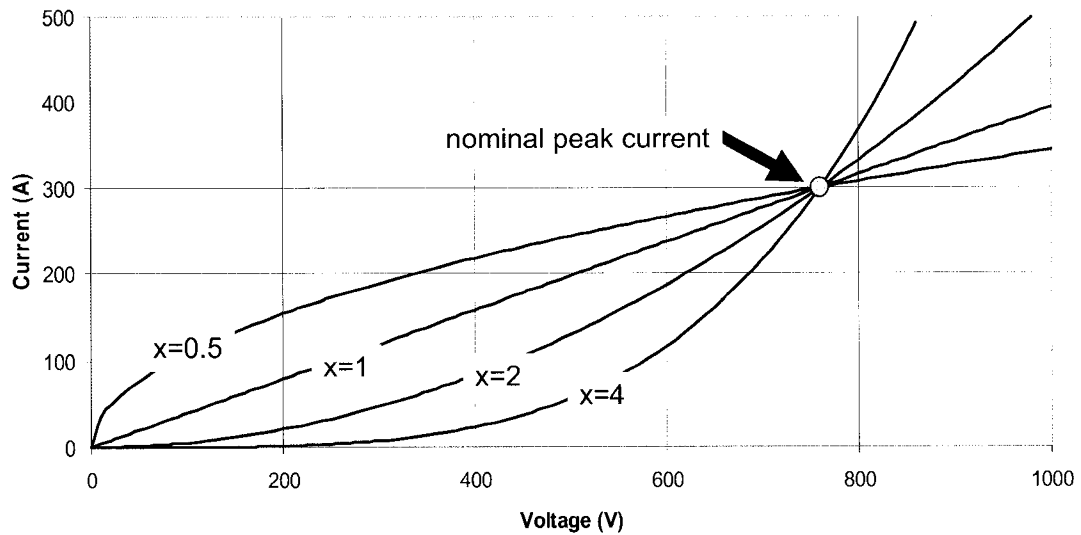

Figure 4.2.3. Characteristics of loads for a range exponents.

In Figure 4.2.3, it can be seen that the curves meet only at the origin and at a unique crossover point, marked as the nominal peak current, meaning the peak current for which the pulse circuit is designed. The feasibility of designing for a load where only the current and voltage at the intended peak current are known will be examined by

Reproduced with permission of the copyright owner. Further reproduction prohibited without permission.

simulating for all four cases. First, the circuit will be configured to allow the capacitor voltage and inductor current to reverse, so the circuit can ring. The circuit used for simulation is shown in Figure 4.2.4. Capacitor C1 starts with an initial condition of 1540 volts. Switch S1 closes at the beginning of the simulation, initiating the discharge through inductor L1 and current source B1. Current source B1 implements the function

$$i_{load} = \psi \left| v_{load} \right|^{x} \frac{v_{load}}{\left| v_{load} \right| + \varepsilon} \tag{4.12}$$

where ε (volts) is positive, non-zero, and very small, on the order of 1×10^{-9} volts, to prevent division by zero during the simulation.

Several circuit elements have little effect on the wave shapes, and are in fact included for numerical stability of the simulation. Resistor R2 is added to provide a small amount of fixed damping, R4 provides a direct current (DC) path to ground for L1 at all times, R1 provides a tiny amount of damping of L1, and R5 essentially sets a minimum impedance across the two nodes. The combination of C2 and R3 provide high frequency damping of the circuit. These measures are necessary to help stabilize the simulation particularly at larger values of x where the non-linearity presented by B1 is more extreme.

Reproduced with permission of the copyright owner. Further reproduction prohibited without permission.

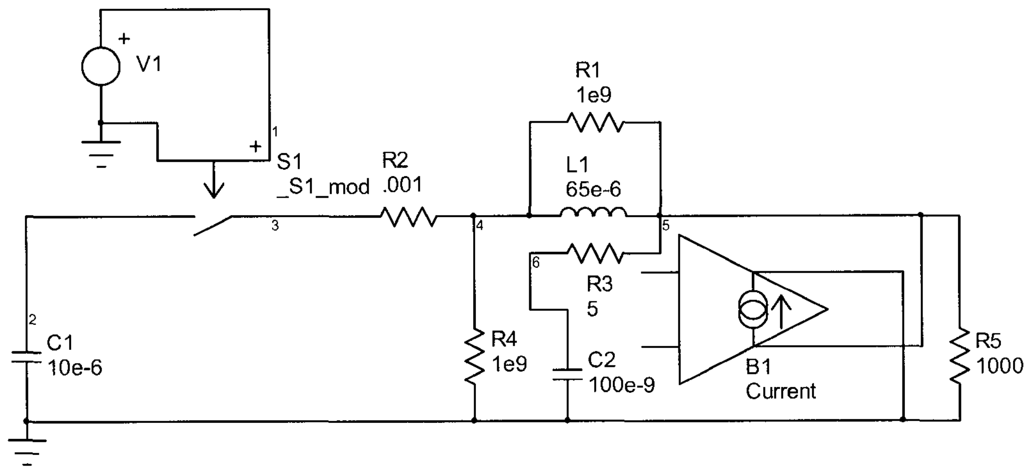

Figure 4.2.4. Circuit for simulation with different loads, allowing ringing.

Simulations were performed with the Intusoft ICAP/4 software package.[7] Results of the simulations for all four values of x are shown in Figure 4.2.5. The peak currents fall within ± 3 % of the midpoint between the lowest and highest peak values. This suggests that it may be reasonable to design the discharge circuit based on matching the large signal impedance at the desired operating point.

Reproduced with permission of the copyright owner. Further reproduction prohibited without permission.

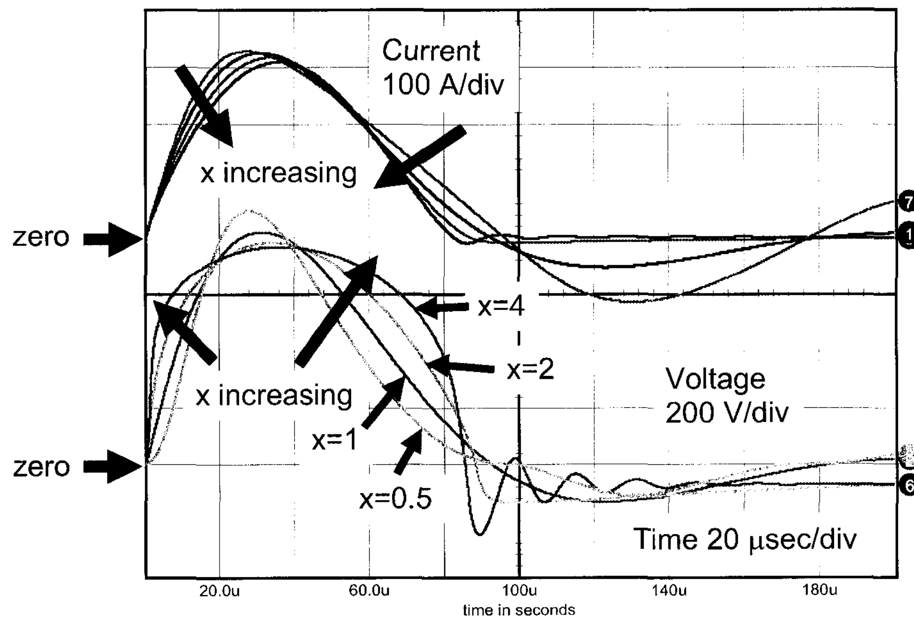

Figure 4.2.5. Waveforms for simulation allowing capacitor voltage reversal.

In actual practice, it is usually undesirable to allow the capacitor voltage to reverse. Implications can include reduced capacitor life and damage to the capacitor charging power supply. Reversal can be prevented by placing a diode in parallel with the capacitor. The circuit used for the simulations is shown in Figure 4.2.6. Diode D1 has been placed in parallel with capacitor C1 to prevent voltage reversal. Other than that, the simulations performed are the same. The resulting waveforms are shown in Figure 4.2.7. An important point to note is that the currents do not reverse. The current waveforms in Figures 4.2.5 and 4.2.7 are essentially identical up to 60 microseconds, then, since the currents do not reverse in Figure 4.2.7, none of the energy in the inductor can go back to the capacitor C1, so the current remains positive until the energy in the circuit is dissipated.

Reproduced with permission of the copyright owner. Further reproduction prohibited without permission.

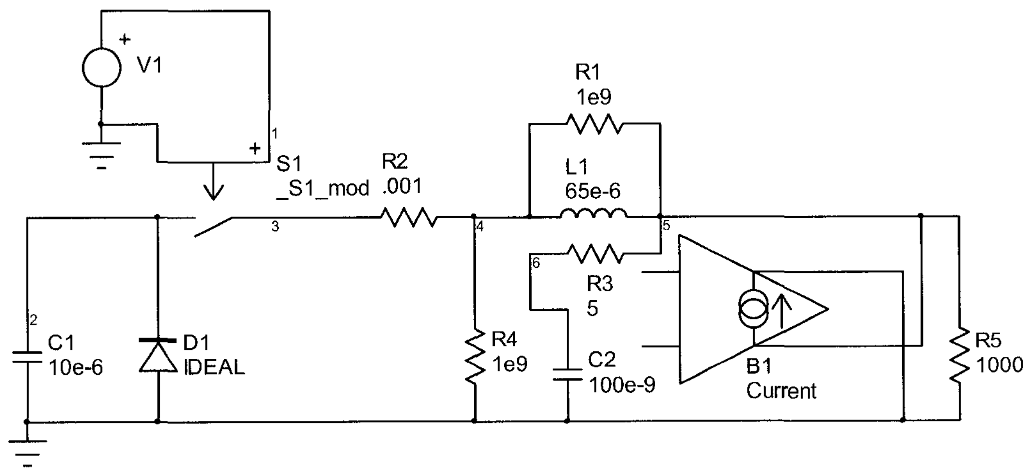

Figure 4.2.6. Circuit for simulation with different loads with diode D1 to prevent capacitor voltage reversal.

Reproduced with permission of the copyright owner. Further reproduction prohibited without permission.

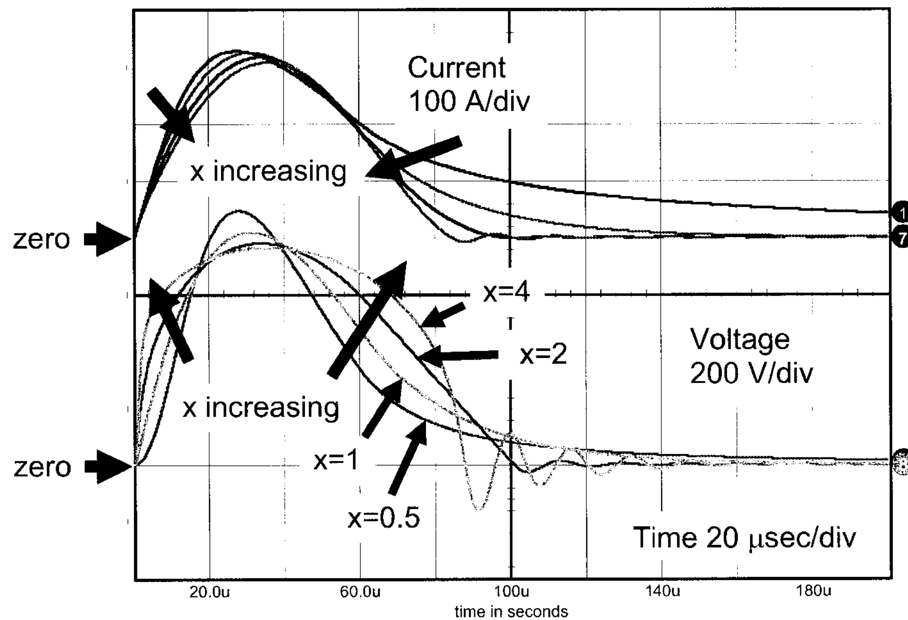

Figure 4.2.7. Waveforms from simulations with capacitor voltage reversal prevented.

This example suggests that it is reasonable to design the discharge circuit assuming a resistive load whose resistance is the same as the large signal impedance of the plasma load at the desired operating point, at least for the other three exponent values examined (the resistive load corresponds to the unity exponent). Simulations showed that for loads where current was an exponential function of voltage, the peak currents fell within a few percent of the resistive load case. Other cases were examined in the course of this research, yielding similar conclusions. It seems that the single mesh PFN seeks to reach its peak current near the matched load condition in examples such as this.

Reproduced with permission of the copyright owner. Further reproduction prohibited without permission.

4.3 Modifications for Arc Handling

It is well known that practical plasma sputtering processes arc at least occasionally, and sometimes heavily. It is necessary to detect and handle arcs for modern sputtering processes to deposit viable films. That is especially true in the case of high power pulsed magnetron sputtering discharges, with considerable stored energy available in the discharge circuit. First, the arc must be detected by some means, then it must be handled. Arc handling can be viewed as having three facets. First, the current must be stopped from rising any further. Second, the plasma load must be disconnected from the power source. Third, the energy stored in the pulse forming network inductor must be moved elsewhere.

There are a number of ways an arc can be detected. Voltage fall may be used to detect an arc. When a low impedance arc occurs at the load, the output voltage will initially collapse to near zero. This is because the discharge circuit consists of an inductor in series with a capacitor. The capacitor has a low impedance in response to a fast edge, but the inductor has a high impedance, allowing the rapid collapse in load impedance concomitant with an arc to pull the output voltage to near zero. The simplest implementation of the voltage fall arc detection logic considers both current and voltage. When the current is above some predetermined threshold level and the voltage falls below a second predetermined threshold, an arc is considered to exist at the load. At that point, the arc handling routine is initiated. Another approach to arc detection is to use current rise as an indication of the arc. A fixed or adjustable threshold can be used. When the current exceeds the threshold, the arc handling routine is initiated. From practical considerations, it is important to have an absolute maximum threshold which is low

Reproduced with permission of the copyright owner. Further reproduction prohibited without permission.

enough to prevent damage to the pulser due to an over current event. The arc detection current threshold can actually be updated on a pulse by pulse basis by predicting the output current, based on plasma load characteristics and the initial value of the voltage on C1 and the values of C1 and L1 and adding margin to prevent false arc detections. The peak output current can be estimated with equation 4.6 as discussed earlier in section 4.2. The arc detection threshold could be set at a margin of perhaps 10% or 20% above the predicted peak current value to prevent false arc trips. Alternately, the current threshold may be adaptively updated based on a moving average of the peak current, with margin added to prevent false arc detections. In this case, it would probably be desirable to leave pulses during which arcs occurred out of the moving average calculation.

The single mesh PFN looks appealing for the discharge circuit, since it meets the stated requirements for the application, including naturally limited peak current and rate of rise and reasonable insensitivity of peak current to output voltage. Now the possibility of modifying the basic discharge circuit to include arc handling will be considered.

The first facet of arc handling is to stop the increase of current. This may be accomplished by disconnecting the capacitor from the inductor. Current rise implies increased energy in the inductor. If the capacitor is disconnected from the inductor, then there is no means to increase its energy, hence current rise will be stopped. The second facet of arc handling is to disconnect the load from the power source. This may be accomplished by placing a switch in series with the output, to disconnect the inductor from the plasma load, while providing a means to clamp the inductor voltage when its connection to the output is interrupted. The third facet of arc handling is to move the energy in the inductor elsewhere. Ideally, the energy in the inductor would be transferred

Reproduced with permission of the copyright owner. Further reproduction prohibited without permission.

to the capacitor with high efficiency. This can be accomplished with a resonant transfer, whose theoretical maximum efficiency is 100%. Dissipation of the inductor energy is undesirable, since a dissipation element must be included in the design, and is likely to be bulky and require cooling.

A circuit capable of the arc handling steps just described is shown in Figure 4.3.1. Four switches are used to first initiate the discharge, and then handle an arc if necessary. Switch S1 initiates the discharge when closed, and stops the increase in inductor current when opened. Switch S2 disconnects the load from the power source when it is opened. Switches S3 and S4 working together connect the inductor L to the capacitor C to resonantly transfer the energy in inductor L at the time of the arc back to capacitor C, where it originated at the beginning of the pulse.

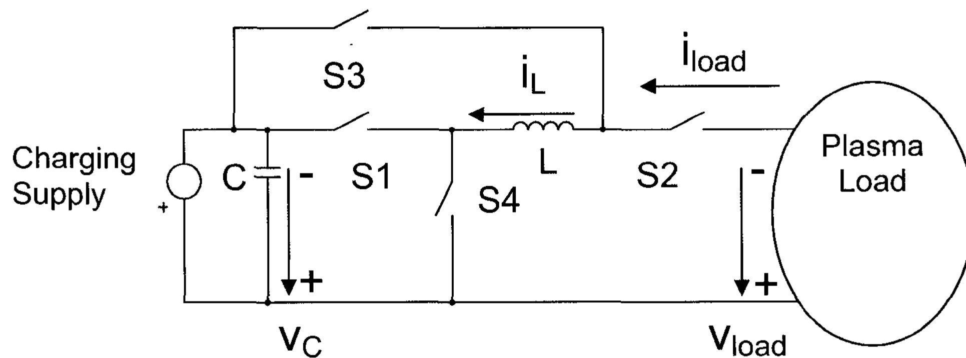

Figure 4.3.1. Pulse discharge circuit with arc handling capability.

Reproduced with permission of the copyright owner. Further reproduction prohibited without permission.

It is possible to use a diode in place of an active switch in some instances. Where possible, this is desirable since the diode essentially switches itself when the circuit requires it to conduct. In Figure 4.3.2, S4 is implemented with a diode, D. The diode, D, automatically conducts current (hence, switches) if S1 is opened while current is flowing in the inductor, L. Otherwise, operation is just as described for the circuit in Figure 4.3.1 above.

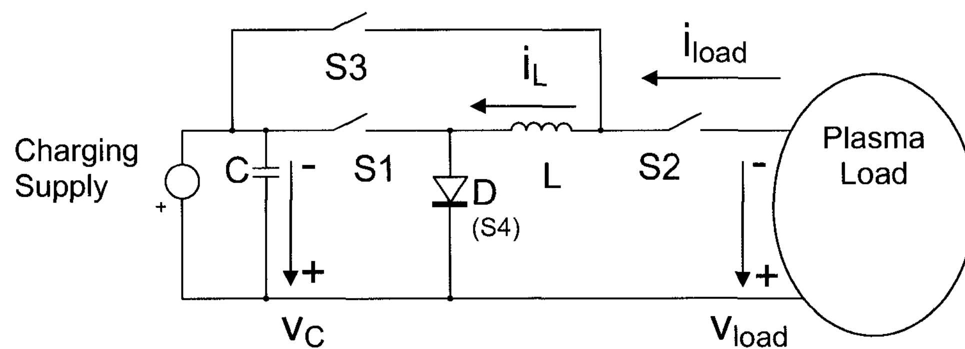

Figure 4.3.2. Pulse discharge circuit with arc handling capability and S4 implemented with a diode, D.

The circuit in Figure 4.3.2 was simulated to in order to validate the arc handling approach just described, especially the concept of recycling the inductor energy to the capacitor. The circuit used for simulation is shown in Figure 4.3.3. It reflects a practical hardware implementation of the circuit shown in Figure 4.2.2. Switches S1, S2, and S3 are voltage controlled switches, controlled by pulsed voltage sources V1, V2, and V3.

Reproduced with permission of the copyright owner. Further reproduction prohibited without permission.

Diode D1 prevents the capacitor voltage from reversing and diode D2 implements switch S4 in Figure 4.3.1, as shown in Figure 4.3.2. Some additions were made for consistency with the constraints of physical implementation. The diodes in parallel with the switches model the anti-parallel diodes required around the thyristor switches used in the experimental pulser. A diode was required in series with S3 in order to prevent undesired conduction through D3. The inductor L2 was added to simulate the inductance of the output cable and process chamber, and diode D5 was added to provide a path for the current in L2 when switch S2 is opened while load current is flowing. Resistor R2 was included to simulate the resistance, albeit low, always present in the physical circuit. Some parts were included for numerical stability. In particular, R4 provides a DC path for L1 and R1 and C2 provide high frequency damping to ensure numerical stability in some situations. A very low impedance, essentially a short circuit, is connected across the output. The simulations were performed with the Intusoft ICAP/4 software package.[5]

Reproduced with permission of the copyright owner. Further reproduction prohibited without permission.

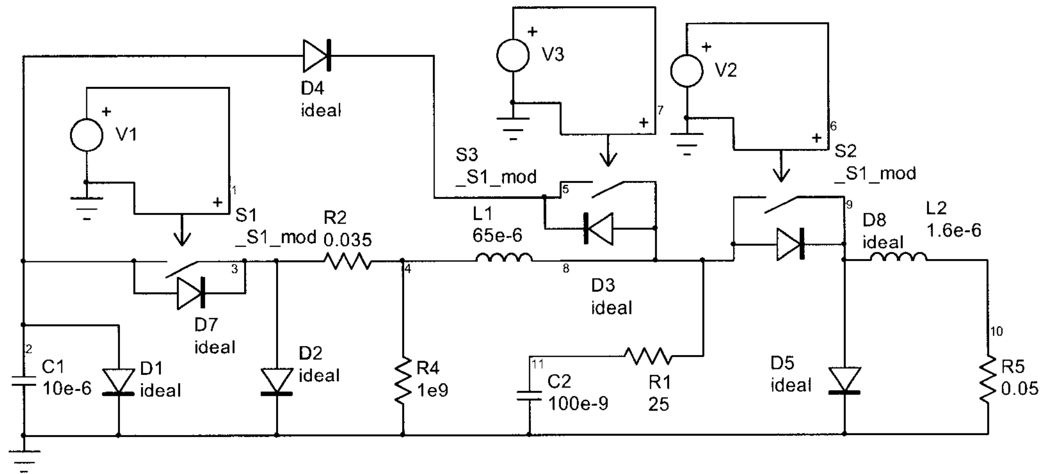

Figure 4.3.3 Simulation circuit diagram for arc handling circuit.

Normal operation of the circuit, with no arc, is the same as for the circuit in Figure 4.2.1, with the exception that the diode D1 prevents the capacitor voltage from reversing, so waveforms would be expected to be similar to those in Figure 4.2.7, where a diode is provided to prevent reversal of the capacitor voltage. This discussion will refer to the component designators (for example, C, D, S1, etc.) used in Figure 4.3.1 and Figure 4.3.2. S2 is closed and S3 is open for the whole sequence. The capacitor C is charged to its initial voltage by the charging power supply in actual operation. For purposes of the simulation, the capacitor is given an initial condition equal to the desired charge voltage. The discharge is initiated by S1, and capacitor C is discharged through inductor L into the plasma load. A control circuit initiates the timing of the switches to control the charge time of the capacitor C and its pulse discharge to the load. The shapes of the v_C, i_L, v_{load},

Reproduced with permission of the copyright owner. Further reproduction prohibited without permission.

and i_{load} waveforms are determined solely by the initial value of v_C, the values of C and L and the characteristics of the plasma load.

Figure 4.3.4 shows waveforms representative of executing the arc handling sequence. In this case, an arc is simulated by a very low impedance, almost a short circuit, connected across the output. The sequence begins as for normal operation, described above, but when the capacitor voltage reaches zero and the inductor current has reached its maximum value, the arc handling sequence is initiated. The discharge is initiated at point "a" when S1 is closed. The current grows to its maximum value which is reached at point "b". At that time, the capacitor voltage reaches zero and diode D (S4) prevents it from reversing. S1 is opened immediately and S3 is closed at point "c" after a short delay of about 8 μsec past point "b". Then S2 is opened at point "d" after another short delay of about 8 μsec past point "c". This disconnects the short circuit load from the output and initiates the resonant transfer of energy from inductor L to capacitor C. The result is that the energy present in inductor L is recycled to capacitor C. The voltage in C rises to near its original value, minus energy dissipated in the circuit resistances and forward voltage drops of the diodes. The inductor is never open circuited when a switch opens in this sequence. If it was open circuit, the voltage across the inductor would increase to a very high value, which would over voltage and damage the opening switch in a physical system.

Reproduced with permission of the copyright owner. Further reproduction prohibited without permission.

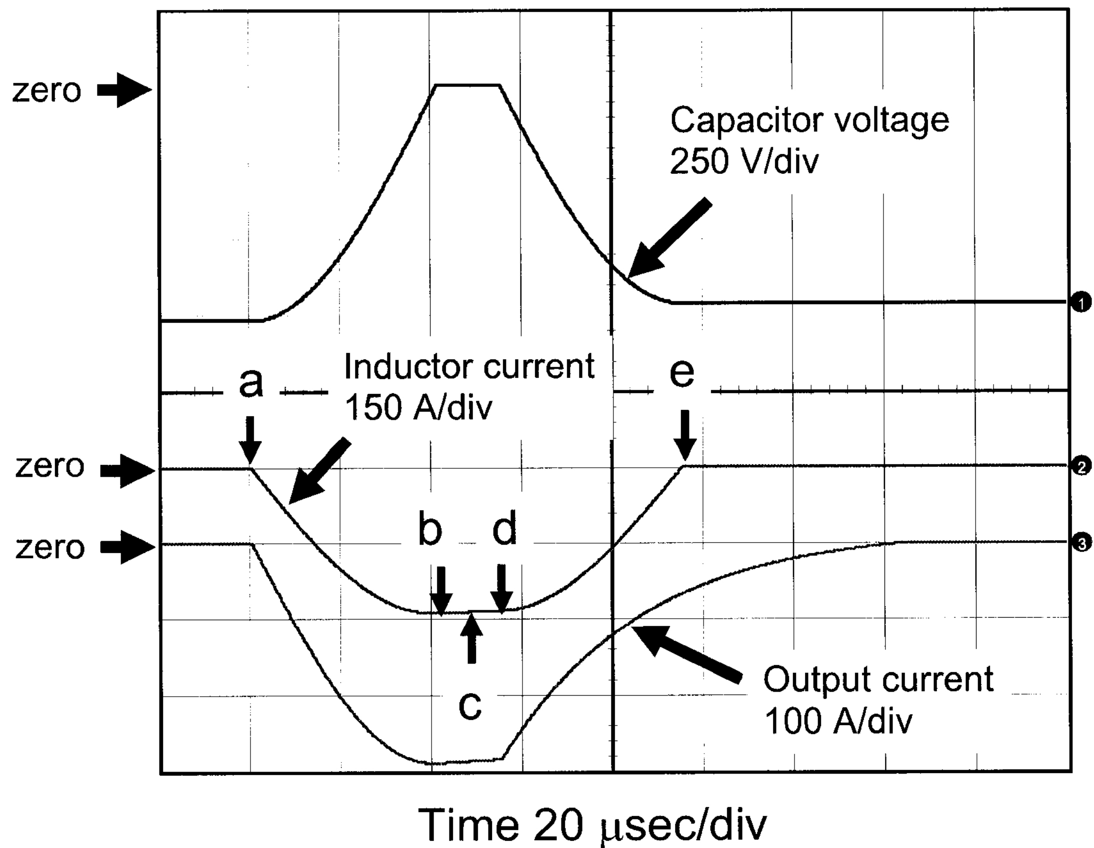

Figure 4.3.4. Simulation results, full discharge.

The case where the capacitor voltage does not reach zero before the arc handling sequence is initiated is shown in Figure 4.3.5. The discharge is initiated by closing switch S1 at point “f”. The current rises until S1 is opened at point “g”. At this point, diode D conducts (S4 closes) to provide a path for the inductor current. Switch S3 is closed at point “h” after a short delay of about 5 μsec past point “g” and then switch S2 is opened at point “i” after a short delay of about 5 μsec past point “h”. The inductor current is steered to the capacitor C, and the inductor current decreases and the capacitor voltage increases as the energy in the inductor is transferred to the capacitor. Again, the final

Reproduced with permission of the copyright owner. Further reproduction prohibited without permission.

capacitor voltage is less than the starting voltage due to the energy dissipated in the circuit.

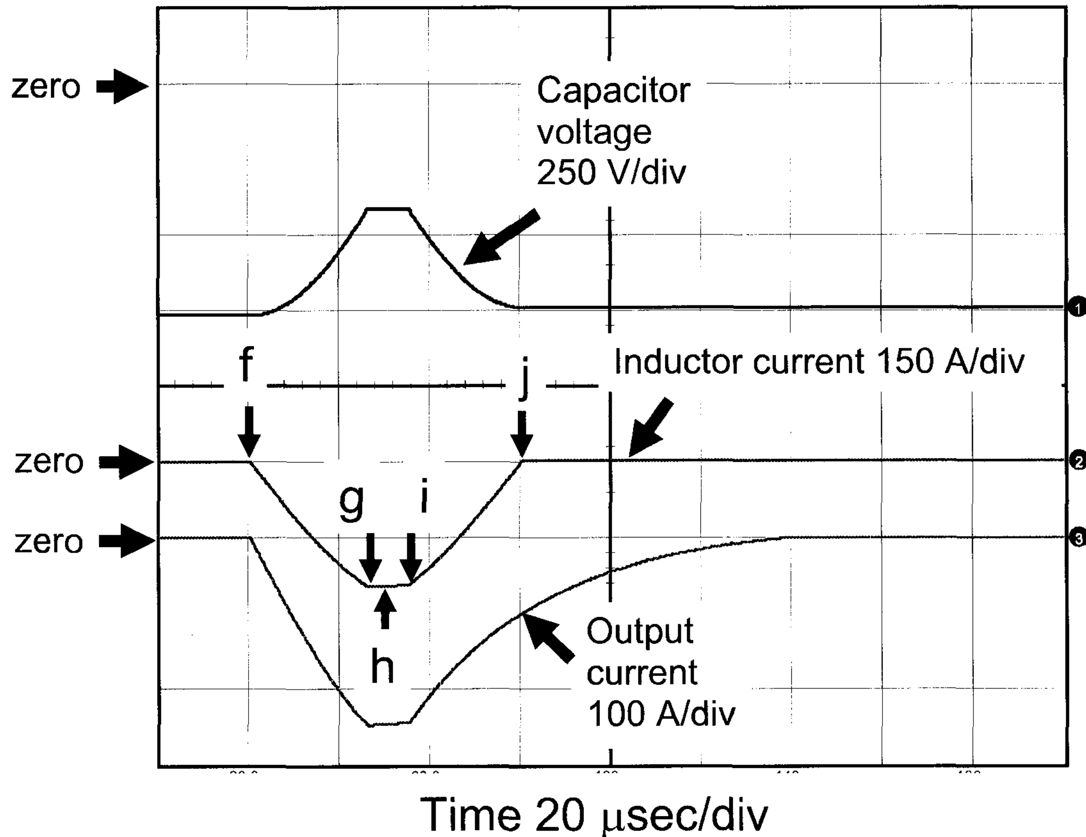

Figure 4.3.5. Simulation results, partial discharge.

A test of the proposed topology, which is new to the best of the author's knowledge, was conducted using actual hardware intended for the final pulser construction. It was operated into a short circuit to allow output current to build up. Then the arc handling routine described above was initiated to disconnect the output from the short circuit, and transfer the inductor energy back to the capacitor. The test setup is

Reproduced with permission of the copyright owner. Further reproduction prohibited without permission.

shown in Figure 4.3.6. The solid state switches are special thyristors, capable of interrupting up to 4000 amperes with a fall time on the order of 1 μsec.[8],[9]

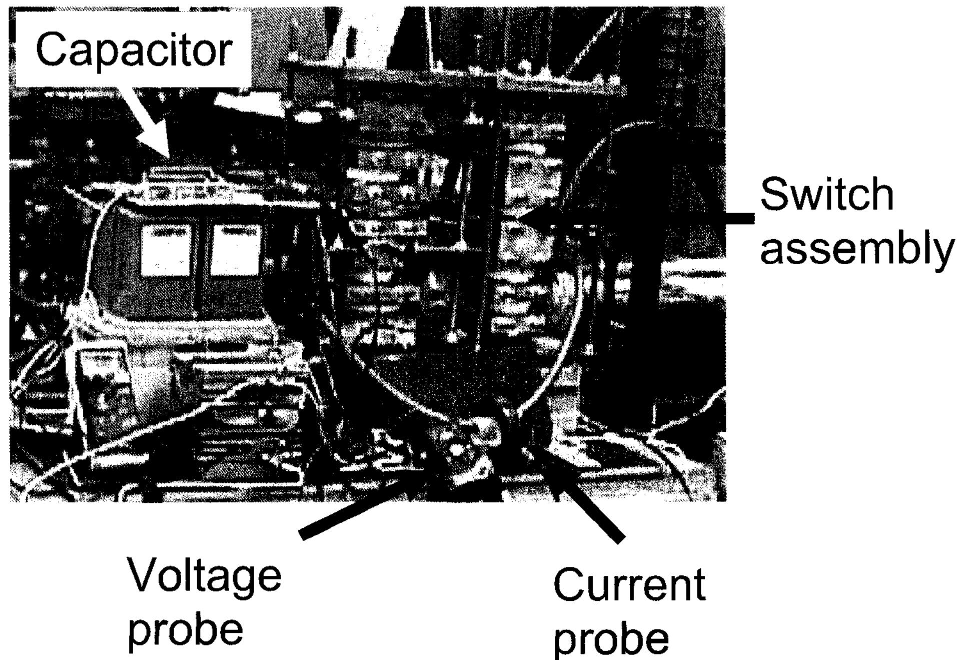

Figure 4.3.6. Topology test setup.

Waveforms obtained from the test are shown in Figure 4.3.7. They are very similar to the waveforms obtained from the simulation, shown in Figure 4.3.4. The simulation was used as part of the design process for the physical circuit, which performed very similarly to the simulation. The simulation was tuned to match the actual circuit by simply incorporating measured or inferred values of L1, L2, R2, R5 and switch timing. No other changes were required to make the simulation match the experiment. The differences between the waveforms are due primarily to small un-modeled parasitic inductances and capacitances, and non-ideal behavior of the thyristor switches. Polarities

Reproduced with permission of the copyright owner. Further reproduction prohibited without permission.

of the test waveforms and simulation waveforms are exactly opposite, due to the conventions used by the simulator and customary conventions used for testing pulsed magnetron supplies. The following discussion refers to the designators in Figure 4.3.1 and Figure 4.3.2. The discharge is initiated at point "a" when S1 is closed. The current grows to its maximum value which is reached at point "b", at that time, the capacitor voltage reaches zero and diode D (S4) prevents it from going negative. S1 is opened immediately and any current flowing in L is conducted by diode D. (Diode D and switches S1, S2, and S3 are made by the same manufacturer. The performance of the switches and diode are matched by design such that the diode is able to turn on and accept current with minimum overshoot at the same rate the switch is shedding current by turning off). Switch S3 is closed at point "c" after a short delay of about 5 μsec past point "b", and then S2 is opened at point "d" after a short delay of about 5 μsec past point "c". This disconnects the short circuit load from the output and initiates the resonant transfer of energy from inductor L to capacitor C. The result is that the energy present in inductor L is recycled to capacitor C. The voltage in C rises to near its original value, minus energy dissipated in the circuit resistance. There was no issue with saturation of the inductor L since it had an air core. The capacitors used were chosen to have a capacitance change in voltage whose magnitude is negligible for this application. The success of this test validates the simulation results and demonstrates the feasibility of implementing the proposed arc handling approach in hardware.

Reproduced with permission of the copyright owner. Further reproduction prohibited without permission.

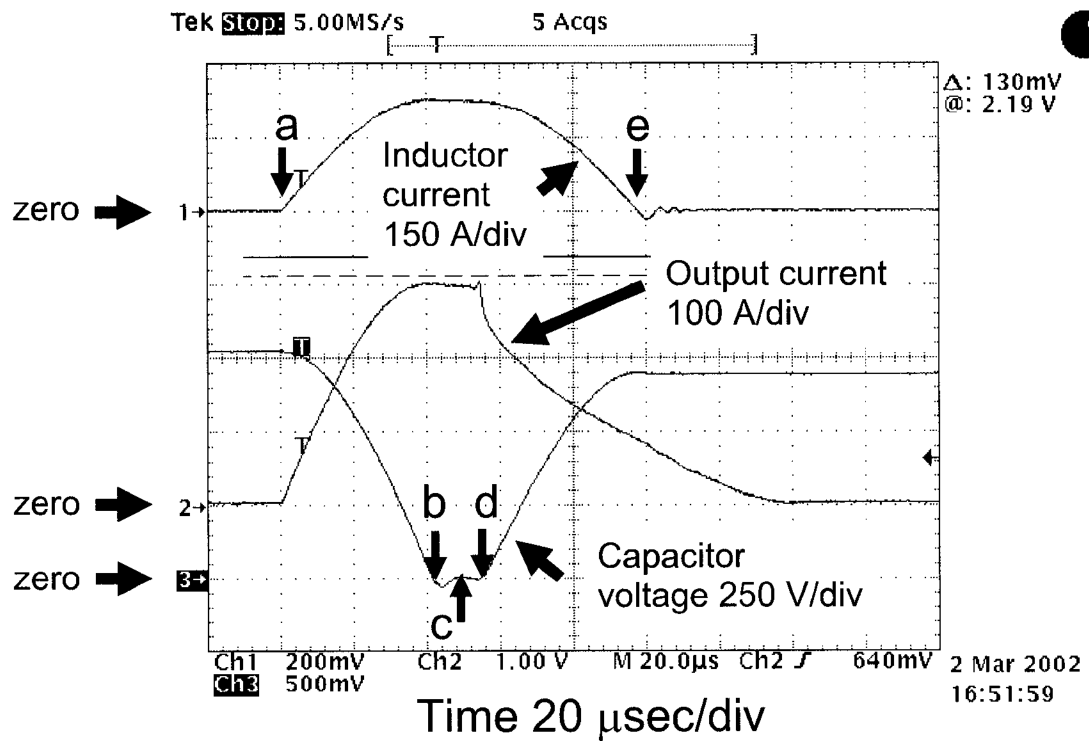

Figure 4.3.7. Topology test waveforms.

4.4 Experimental Conditions

An experimental pulsed power supply for HPPMS was built based on the principles discussed so far in this chapter. The operating capabilities of the power supply are: pulse width nominally 100 to 150 μsec, pulsing frequency single shot to 500 Hz, PFN characteristic impedance 0.5 to 3.0 Ω, capacitor charging voltage 500 to 3000 V, pulse current up to 3200 A, and average power in excess of 15 kW. The unique feature of this capacitor discharge power supply is arc handling, which is a key technology for the practical application of HPPMS to industrial processes.

The experimental pulsed supply system is shown in Figure 4.4.1. The pulser rack holds the high power switch assembly, discharge capacitor bank, and discharge inductor.

Reproduced with permission of the copyright owner. Further reproduction prohibited without permission.

The high power switch assembly includes all of the high power switches and diodes in the discharge circuit with arc handling capability shown in Figure 4.3.2. Selectable discharge capacitance is provided by the capacitor bank. The capacitance can be varied from 10 μF to 60 μF in 10 μF steps. The discharge inductor has several taps, with choices ranging from about 20 μH to 120 μH. An ignition circuit is also incorporated in the pulser rack. It is essentially a small capacitor, less than 1 μF, in series with a few ohm resistor. The capacitor forms a ringing circuit with the discharge inductor, which results in a well defined voltage overshoot when operated into an open circuit, such as a plasma chamber prior to ignition. This voltage overshoot helps to ignite the plasma. The resistor serves to damp the ringing of the output voltage and also to set the magnitude of the voltage overshoot. With no damping resistor, the voltage would overshoot to twice the discharge capacitor charge voltage. With heavy damping, overshoot could be eliminated. An intermediate approach, employed here, is to choose the resistor such that the voltage overshoot reaches about one and a half times the charge voltage, and the ignition waveform rings for just a few cycles. The control chassis provides power and control signals to the pulser rack. It generates the signals required to control the high power switches for both typical pulse discharges and for the arc handling sequence. Switch control signals are transmitted to the pulser rack over fiber optic cables. The control chassis incorporates the logic circuitry required to detect arcs based on both current rise and voltage collapse, and to perform the arc handling sequence. The capacitor charging supply is a 3 kilovolt ion source power supply which has been modified for capacitor charging service. Repetitive capacitor charging typically requires that the power supply first operate at its current limit, and then at its power limit, until the charge voltage set

Reproduced with permission of the copyright owner. Further reproduction prohibited without permission.

point is reached. At that point, the power supply must shut off essentially instantaneously. Then, when the capacitor is discharged, the power supply must automatically re-charge the capacitor as just described. The experimental pulsed power system has operated flawlessly, with no failures, for more than fifteen months.

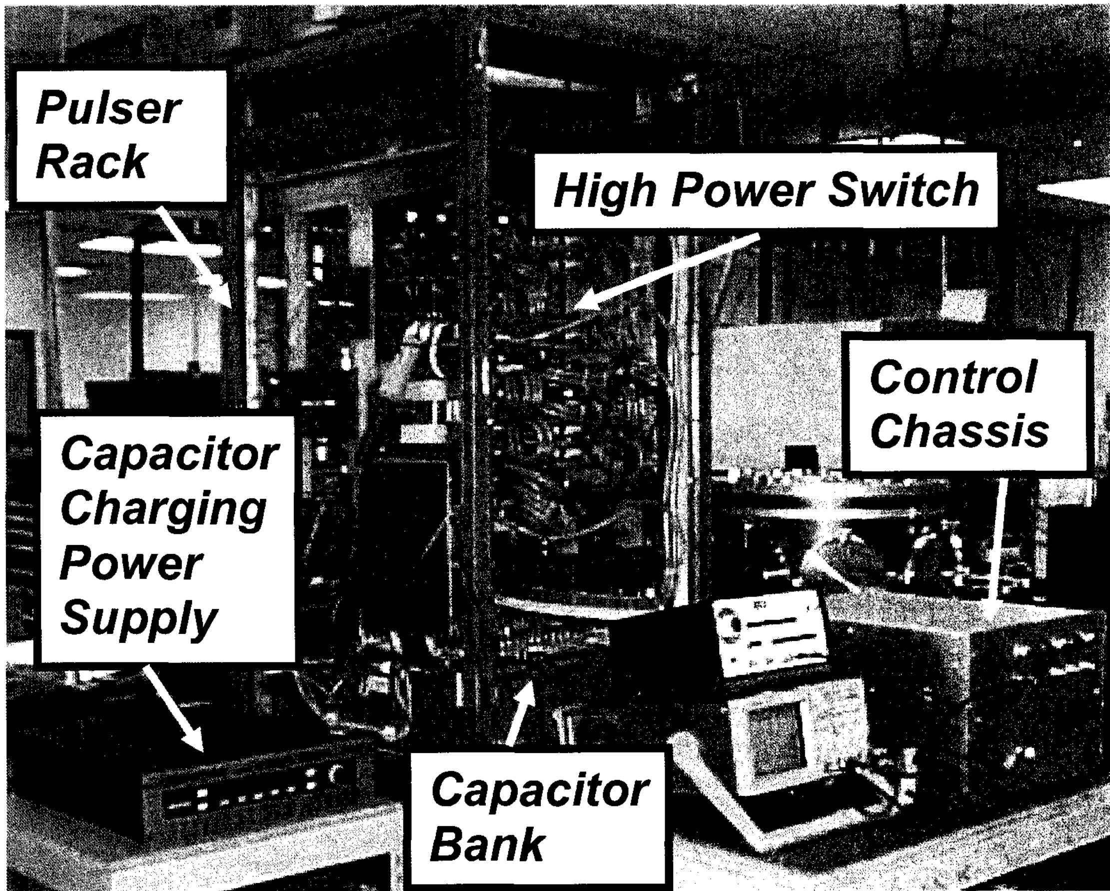

Figure 4.4.1. Experimental HPPMS pulsed power supply system.

Data were generated in two separate systems. Lower current data were generated with a medium sized, cylindrical (0.76 m diameter x 0.46 m deep) vacuum chamber with a single 0.15 m Torus 10 balanced-field magnetron fitted with an aluminum target. High

Reproduced with permission of the copyright owner. Further reproduction prohibited without permission.

current data were generated with a larger volume (1.22 m x 0.91 m x 0.76 m) chamber with a 0.30 m x 1.12 m planar magnetron fitted with an aluminum target. Process gas flow was controlled with mass flow controllers. Both chambers were turbo-molecular pumped to base pressures below 7×10^{-4} Pa (5×10^{-6} Torr) prior to experimental runs.

4.5 Results and Discussion

Initial plasma testing was accomplished on the large magnetron with the pulser configured for a nominal 0.5 Ω impedance. The objective of these initial tests was to verify operation of the pulser driving a magnetron at high peak power and close to maximum average power. Both plasma ignition and arc handling were evaluated in these tests. Waveforms for a typical pulse with no arcing are shown in Figure 4.5.1. In particular, there is no sign of arcing at the beginning of the pulse. The voltage never collapses to near zero (or, a few tens of volts), which would be an observed effect of an arc. A built in ignition circuit provides a voltage overshoot at the beginning of the pulse which serves to ignite the plasma. It consists of essentially a small capacitor in parallel with the pulser output. The capacitor rings with the discharge inductor to generate a peak voltage higher than the initial discharge capacitor voltage. The resistor damps the ringing, and also serves to limit the peak amplitude of the initial voltage spike. The peak current of the pulse was 1350 A at a discharge voltage of 500 V, corresponding to a peak power of about 675 kW. The initial voltage waveform rings at a frequency of about 50 kHz and the amplitude of the ringing decreases quickly due to the resistive damping built in to the ignition circuit. Power density in this case is estimated at 0.5 kW/cm^2, which is approaching the 1 kW/cm^2 level where the onset of significant ionization is expected to

Reproduced with permission of the copyright owner. Further reproduction prohibited without permission.

occur.[1,5,6,10] Peak power and magnetron target area are used to estimate power density. The entire magnetron area was used, because at high peak powers, the magnetron plasma tends to spread and cover the surface of the magnetron target. Waveforms of the power supply responding to an arc at the same process conditions are shown in Figure 4.5.2. When the arc occurs the voltage falls, but current stays relatively constant. The arc occurs at the peak current in this case, however, arcs were observed to occur at almost any temporal position within the pulse. The major point of testing on this large magnetron was to verify the ability of the pulser to light and drive a magnetron plasma at high current, and to handle arcs occurring during high peak power operation of the magnetron.

Reproduced with permission of the copyright owner. Further reproduction prohibited without permission.

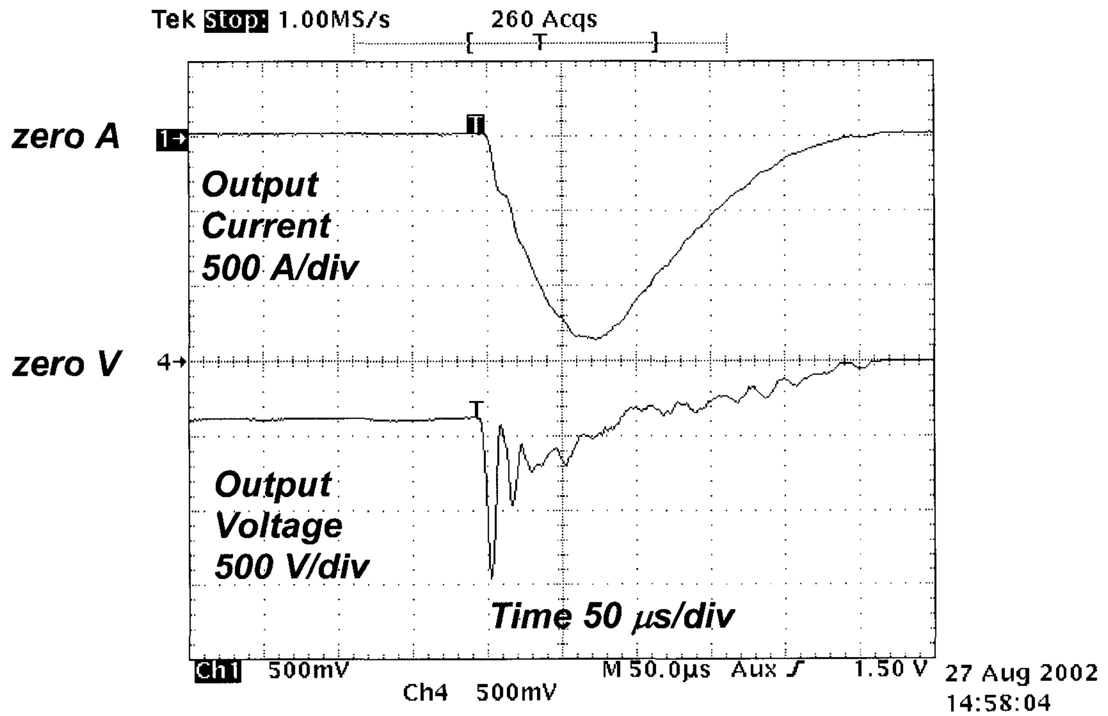

Figure 4.5.1. Oscilloscope photo of typical operation into a large (0.30 m by 1.12 m) magnetron.

Reproduced with permission of the copyright owner. Further reproduction prohibited without permission.

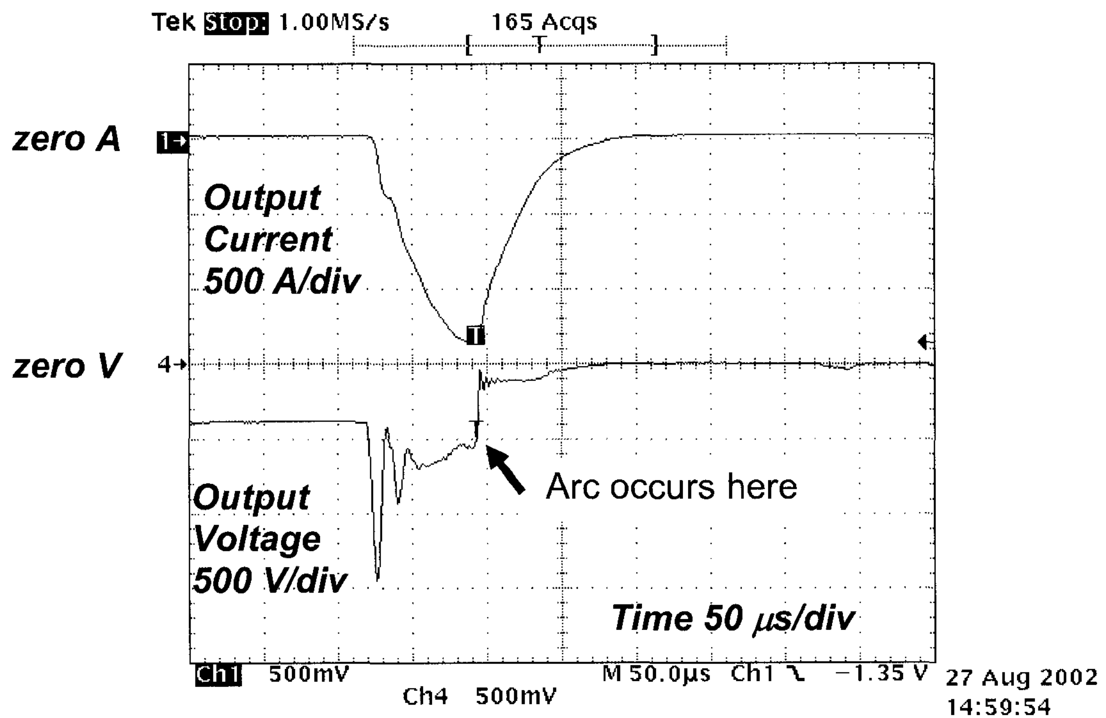

Figure 4.5.2. Oscilloscope photo of arc handling into a large (0.30 m by 1.12 m) magnetron.

Additional testing was performed with the Torus 10 magnetron. In this case, the pulser was configured for a nominal 3.0 Ω impedance. Waveforms for typical operation at lower current are shown in Figure 4.5.3. Again, there is no sign of an arc at the beginning of the pulse, since the voltage never collapses to near zero, or a few tens of volts. The peak current of 450 A occurs at a discharge voltage of 900 V corresponding to a peak power of 400 kW. This corresponds to a power density of 2.5 kW/cm^2, well above the 1 kW/cm^2 level where significant ionization is expected to occur.[1,5,6,10] Power density was estimated using peak power and magnetron target area, since the plasma was observed to spread over the whole surface of the target. The surface wear (so called

Reproduced with permission of the copyright owner. Further reproduction prohibited without permission.

"racetrack") pattern on the magnetron target also indicated that sputtering occurred over the entire surface of the target. Arc handling waveforms at the same process conditions are shown in Figure 4.5.4. The voltage falls when the arc occurs, however, in this case, the current jumps. This current jump is attributed to energy in the ignition circuit capacitance being discharged into the arc through the ignition circuit damping resistor.

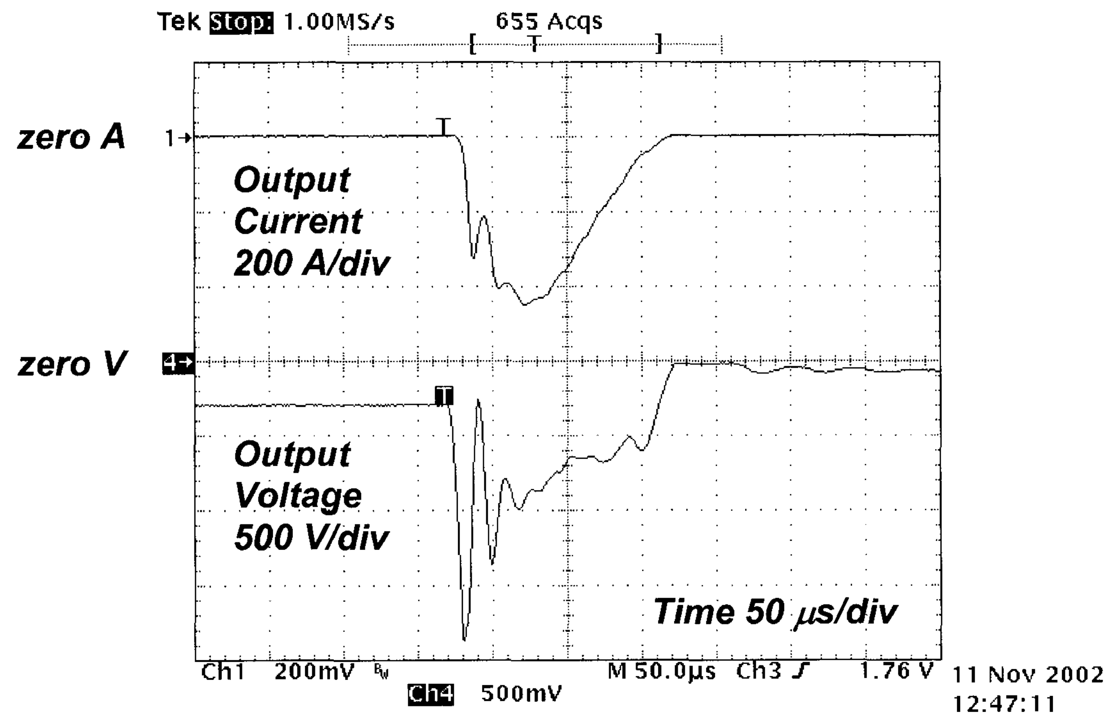

Figure 4.5.3. Oscilloscope photo of normal operation into small (0.15 m) magnetron.

Reproduced with permission of the copyright owner. Further reproduction prohibited without permission.

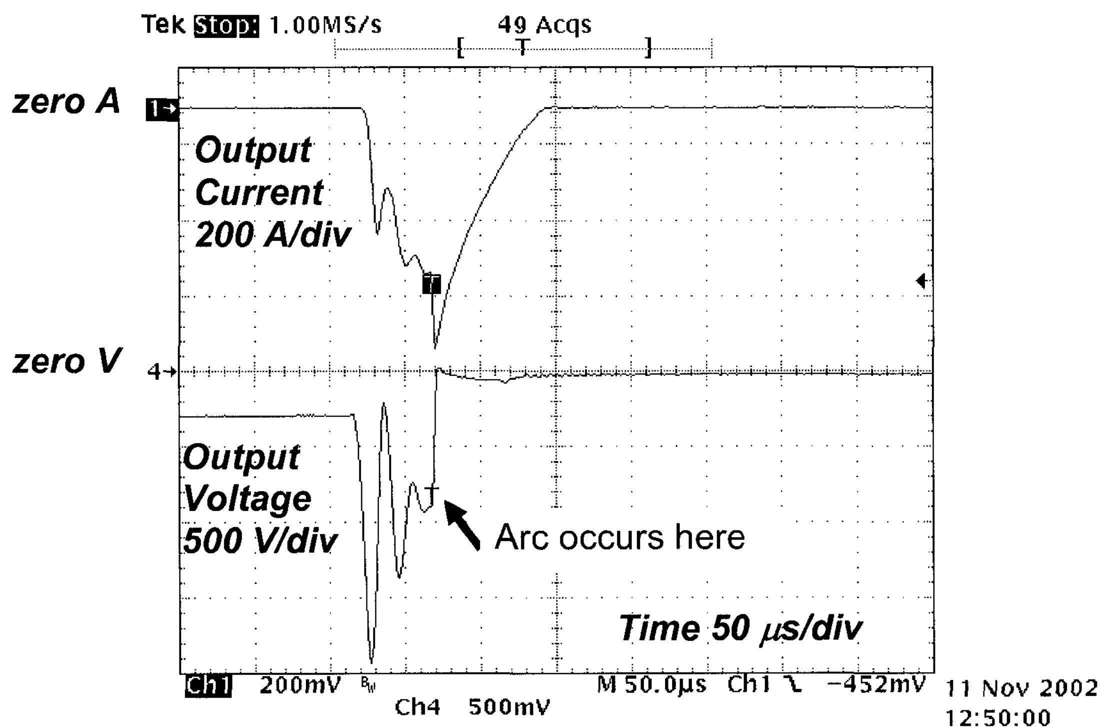

Figure 4.5.4. Oscilloscope photo of arc handling into small (0.15 m) magnetron.

4.6 Process Results Enabled by the Experimental Pulsed Power Supply

In addition to laboratory tests of the power supply, collaborative efforts were undertaken to explore the ability of this power supply to enable new thin film deposition process capabilities. These efforts involved integration of the pulser into deposition systems at remote facilities. The experiments performed in these campaigns showed that the pulser described herein can enable HPPMS processes not possible without arc handling.

One important application is thin tribological and corrosion protection films for hard disk rotating media. As the storage density increases, the spacing between the

Reproduced with permission of the copyright owner. Further reproduction prohibited without permission.

magnetic part of the head and media necessarily decreases. This drives all of the layers to be thinner. For next generation media, it is anticipated that even thinner carbon films will be required. In order to provide the same anti-corrosion performance, the density of the films must increase. It was an object of this research to create thin carbon films with high density using essentially conventional magnetron sputtering equipment.

Results were reported by DeKoven et al.[1] In summary, deposition of thin (< 20 nm) films with HPPMS using carbon cathodes in a 6-inch circular magnetron was described. Evidence for increased plasma ion production compared to continuous D.C. magnetron sputtering was presented, using both plasma emission spectra and a gridded quartz crystal microbalance (QCM). The fraction of the ions consisting of C was estimated to be on the order of 5% based on gridded QCM measurements which assumed only C and C^+ were present. This assumption was based on optical emission spectroscopy of the plasma.[1] Carbon film densities up to 2.7 g/cm^3 were measured by a commercial analytical laboratory using x-ray reflectivity (XRR) techniques. Film density was significantly increased compared to films deposited by PECVD (2.1 g/cm^3) or D.C. sputter deposition (< 2.0 g/cm^3), attributed to atomic peening by primarily Ar^+ ions produce by the dense plasma, although C ions may contribute to the higher density as well. The resulting carbon films were graphite-like with estimated sp^3 fraction in the range 0.20 – 0.30, measured by a commercial analytical laboratory. Electron microscopy to assess microstructure of the films has not yet been performed. RMS roughness of the HPPMS films was 0.57 nm as opposed to 1.4 nm for the DC films, attributed to atomic peening in the HPPMS process.

Reproduced with permission of the copyright owner. Further reproduction prohibited without permission.

Deposition of carbon by HPPMS was demonstrated for the first time known to the author. The deposition process achieved densities 40% higher than reported for DC sputtered carbon.

In the second collaborative effort, the pulser was applied to a reactive sputtering process in an inline glass coater with cylindrical rotating magnetrons.[2] The first significant accomplishment was HPPMS operation of a large area reactive sputtering process depositing TiO_2 films on glass, a dielectric film on a dielectric substrate material, for the first time known to the author. In addition, operation of the process in the transition mode was achieved by partial pressure regulation with the IRESS control system.[11] Arc handling, combined with partial pressure regulation, enabled this reactive sputtering process to operate in the transition region while reactively depositing dielectric film on a dielectric substrate. Pulses of 0.5 – 1 MW at a frequency of 100 – 500 Hz were used to reactively sputter TiO_2 from a metallic target. Higher indexes of refraction were observed for HPPMS than for DC, but deposition rates were lower, on the order of 30% of the DC rate. Higher indexes of refraction are expected to correlate to higher densities of the deposited film. A detailed explanation for the reduction in rate is still open, however, it seems possible that a significant fraction of the ionized target material could be transported back to the target, rather than to the work piece.

These two collaborative efforts showed that HPPMS power supplies with arc handling, combined with essentially conventional magnetron sputtering sources, can enable a new range of deposition processes. The investigations summarized here represent just a small sample of the application possibilities.

Reproduced with permission of the copyright owner. Further reproduction prohibited without permission.

4.7 Summary

A novel power supply for HPPMS incorporating arc handling has been designed and built. Plasma ignition and arc handling has been demonstrated on magnetrons with aluminum targets at currents up to 1350 amperes. Well established pulse power principles applied to the basic discharge circuit design have been described, as well as a new example suggesting the validity of designing to simply match the load to the large signal impedance. New techniques for arc handling with a single mesh PFN were developed to handle unavoidable process arcs. Arc handling enabled operation on a magnetron with an aluminum target at a power density of 2.5 kW/cm^2 and has been shown to enable HPPMS deposition of materials such as carbon and HPPMS transition mode reactive deposition of dielectrics on insulating substrates. It is anticipated that the novel pulsed power supply reported herein will enable the future HPPMS deposition of even more materials in both metallic and reactive sputtering processes.

4.8 References

[1] B. M. DeKoven et al., Soc. of Vac. Coaters 46th Annual Tech. Conf. Proc., 158 (2003).
[2] J. Davis et al., to be published in the Soc. of Vac. Coaters Annual Tech. Conf. Proc.
[3] G. N. Glasoe and J. V. Lebacz, Pulse Generators (McGraw-Hill, New York, 1948).
[4] J. P. Markiewicz, J. L. Emmett, J. Quantum Elec. QE-2, 707 (1966).
[5] V. Kouznetzov et al., Surf. and Coatings Technol. 122, 290 (1999).
[6] A. P. Ehiasarian, et al., Vacuum 65, 147 (2002).
[7] www.intusoft.com.
[8] H. E. Gruening, A. Zuckerberger, IEEE Ind. Applic. Soc. Conf. Record, 1474 (1996).
[9] S. Bernet et al., IEEE Trans. on Ind. Applic. 35, 487 (1999).
[10] K. Macák et al., J. Vac. Sci. Technol. A 18, 1533 (2000).
[11] W. D. Sproul, B. E. Sylvia, Vac. Technol. and Coating, 32 (Aug. 2001).

Reproduced with permission of the copyright owner. Further reproduction prohibited without permission.

CHAPTER 5

SUMMARY AND FUTURE WORK

5.1 Perspective

The research presented in this dissertation addresses three facets of reactive sputtering technology. First, a methodology for quantitative understanding of the process driven requirements for power supply shutdown in response to an arc was developed. Second, modeling was employed to show that regulation of the reactive gas partial pressure is required to gain control of film composition and deposition rate in reactive co-sputtering. Experiments showed that changing just the reactive gas partial pressure can result in a change of composition and deposition rate. Third, an understanding of the general requirements for HPPMS power supplies was developed. Then, a topology was developed to add arc handling capability to capacitor discharge HPPMS power supplies. A collaborative effort demonstrated HPPMS reactive deposition of dielectric films on dielectric substrates, enabled by an HPPMS power supply with arc handling, for the first time known to the author.

5.2 Reactive Sputtering Arc Response Dynamics

The requirements for power supply arc response time were examined quantitatively for a specific system and reported for the first time known to the author. The methodology employed includes design of a stabilizing controller. Although reactive sputtering

Reproduced with permission of the copyright owner. Further reproduction prohibited without permission.

controller designs have been reported since at least 1980, this is the first time to the author's knowledge that the approach of Jacobian linearization and linear quadratic regulator (LQR) design as a starting point have been reported. The groundwork has been laid for more exotic controller designs, and greater understanding of the reactive sputtering process. A suggestion for future work is to focus on understanding the implications of arc response more globally. In this research, a specific system was studied. Next, it may be possible to characterize a system in terms of parameters analogous to aspect ratios. Some examples of potentially useful parameters are target area to chamber area ratio, and chamber volume to chamber area ratio, or the ratio of target material to compound sputtering yield. With this approach, it may be possible to produce general results, perhaps presented as a set of design curves, which are useful for a wide variety of system configurations.

5.3 Pulsed Reactive Co-Sputtering

The reactive co-sputtering process has been explored by modeling. Key results show that regulation of the power to each target and partial pressure regulation are required in order to gain control over both film composition and deposition rate. Experiments were performed to demonstrate that changing just the partial pressure can result in a change of film composition and deposition rate.

A suggestion for future work is to develop a dynamical model of the reactive co-sputtering process, accounting for cross-coupling of the plasma between the two magnetrons if required. More advanced applications may require control systems which enable controlled variation of composition with time, hence allowing the index of

Reproduced with permission of the copyright owner. Further reproduction prohibited without permission.

refraction to be changed as a function of thickness. This would enable reactive co-sputtering deposition of so-called rugate optical filters, where the index of refraction is varied periodically with thickness for several cycles to obtain the desired spectral response. A dynamical model would allow a control system to be implemented accounting for process dynamics, enabling tracking of a desired composition reference input. If the composition reference input were varied with time, and the deposition rate could be estimated or measured, then the index of refraction could be varied with thickness in a predetermined manner. At a minimum, such a model would be a major aid in the design of the partial pressure regulation loop.

5.4 HPPMS Power Supplies for Reactive Sputtering

The basic theory of designing capacitor discharge circuits for plasma loads was reviewed, then it was shown by simulation that these designs can be relatively insensitive to the exponent, x, in cases where

$$i \propto v^x \tag{5.1}$$

where i (amperes) is current and v (volts) is voltage. Next, a novel topology which adds arc handling with inductor energy recycling to the basic discharge circuit was proposed and verified by simulation and experiment.

An experimental pulser capable of arc detection and handling was constructed and its performance was verified on two magnetron plasma loads, one large (0.30 m by 1.12 m) and one small (0.15 m diameter). Following initial testing, the pulser was used in collaborative research efforts where it demonstrated that the addition of arc handling to an HPPMS power supply can enable interesting new thin film deposition processes. In

Reproduced with permission of the copyright owner. Further reproduction prohibited without permission.

particular, the pulsed supply was used to deposit dense (2.7 g/cm^3) thin (< 200 Å) carbon films, and for reactive deposition of dielectric films on dielectric substrates.

A suggestion for future work is to focus on developing applications for HPPMS in the general areas of data storage, tribological coatings, and tool coatings where ionized metal physical vapor deposition (iPVD) is advantageous. It is anticipated that deeper understanding of applications will drive additional research in power conversion and process control specific to HPPMS.

5.5 Integration of HPPMS, Reactive Co-sputtering, and Arc Response Dynamics

A final suggestion for future work is to explore integration of the research presented here in the areas of HPPMS, reactive co-sputtering and arc response dynamics. High density plasma from HPPMS can result in a significant flux of ions to the substrate, whose energy may be controlled by a substrate bias power supply. This has the promise of depositing dense equi-axed films. By invoking co-sputtering, a wide variety of useful film compositions is possible. Adding the possibility of chemistry, based on a wide range of gases, could provide an even wider range of compositions. The use of partial pressure regulation could allow stabilization of both composition and deposition rate when reactive chemistry is employed. Modeling of arc response dynamics will suggest a maximum arc response off time, and, in the case of HPPMS, perhaps a minimum pulse frequency as well.

It seems quite possible that HPPMS with arc handling, integrated with reactive gas partial pressure regulation, in a co-sputtering arrangement, can produce new films with useful properties. First, HPPMS has been shown to deposit denser films than

Reproduced with permission of the copyright owner. Further reproduction prohibited without permission.

conventional sputtering, without the macro-particles characteristic of cathodic arc processes. Production of ionized target material, as well as process gas ions, allows the control of film properties, such as stress, density, and conductivity, with appropriate choice of the workpiece electrical bias. Second, the addition of co-sputtering provides a wide range of composition possibilities. Third, chemistry with reactive gases ranging from O_2 or N_2 to more complex gases, such as hydrocarbons, makes the range of possible compositions even wider. These three considerations suggest the possibility of useful new film processes from the integrated approach offered here.

Reproduced with permission of the copyright owner. Further reproduction prohibited without permission.

APPENDIX A

EXPONENTIAL VOLTAGE – CURRENT CHARACTERISTIC SIMULATION

It has been fairly common to view the plasma load current as proportional to an exponential function of voltage, at least in a limited region of the operating parameter space. It is desired to simulate the function where the current i_{load} (amperes) is expressed as

$$i_{load} = \psi v_{load}^{x} \qquad \text{(A.1)}$$

where ψ (amperes/volt^{x}) is the proportionality constant, v_{load} is the voltage at the plasma load, and x is the exponent to which the load voltage is raised. Simulation will allow candidate drive circuits to be studied and evaluated prior to construction. The simulation package used for these simulations[1] offers a programmable voltage controlled current source which allows the user to write an arbitrary expression for current as a function of voltage. However, there are some constraints which must be met. These constraints preclude the simple use of equation A.1. First a number being raised to an exponent must be non-negative. Since v_{load} can take on negative values, the absolute value of v_{load} must be taken before it is raised to the exponent x, as in equation A.2. The sign of the current must match the sign of the voltage. The sign is determined by dividing v_{load} by its absolute value plus a very small positive constant ε to prevent division by zero when v_{load} goes to zero.

Reproduced with permission of the copyright owner. Further reproduction prohibited without permission.

The current source is programmed to implement the function

$$i_{load} = \psi |v_{load}|^{x} \frac{v_{load}}{|v_{load}| + \varepsilon} \qquad \text{(A.2)}$$

where ε (volts) is positive, non-zero, and very small, on the order of 1×10^{-9} volts, just large enough to prevent division by zero during the simulation. Equation A.2 provides a reasonable approximation of equation A.1, which also meets the requirements of the programmable voltage controlled current source in the circuit simulation package.[1]

[1] Intusoft ICAP/4, www.intusoft.com

Reproduced with permission of the copyright owner. Further reproduction prohibited without permission.